One-dimensional apodization of light beams by the optimized quasi-Gaussian profiles in potential application to lighting the acousto-optical cells with appreciable linear acoustic losses

Principal contributors:

Alexandre S. Shcherbakov [(1)], Daniel Sanchez Lucero [(1)], Ana Virginia Hanessian de la Garza [(1)], and Alexander Laskin [(2)].

1) National Institute for Astrophysics, Optics, and Electronics (INAOE), Puebla, Mexico.
2) AdlOptica GmbH, Berlin, Germany.

Associated contributors:

Abraham Luna Castellanos[(1)], Eduardo Tepichin Rodriguez[(1)], and Sandra E. Balderas Mata[(1)].

National Institute for Astrophysics, Optics, and Electronics (INAOE),

Puebla, Mexico.

Department for Optics, INAOE

Technical report

Index

1. Introduction……..……3

2. Linear acoustic waves and their attenuation……..……4
2.1. Linear elastic waves in solids…….....4
2.2. Linear acoustic attenuation…….....6
2.3. The Akhieser's mechanism of losses for the coherent elastic waves……..……...7
2.4. Effect of linear acoustic attenuation along a distance elastic wave propagation……..…11

3. Analysis of the apodization for light beams by the optimized quasi-Gaussian profiles; application to the acousto-optical cells with appreciable acoustic losses……..……..13
3.1. Introductive remarks……..……...13
3.2. Effect of acoustic attenuation along the aperture of Bragg acousto-optical cell……..……15
3.3. Gaussian apodization of the incoming light field distribution along an aperture of the acousto-optical cell with acoustic losses……..16
3.4. Shifted Gaussian apodization of the incoming light field distribution along an aperture of the acousto-optical cell with acoustic losses…….……18

4. Experimental characterization for the apodization of a light beam by variable Gaussian profiles…….……21
4.1. A multi-prism light beam expander…….……21
4.2. Properties of the beam expander within operating over elliptically polarized light…….……23
4.3 Practical examples for operating over mutually conjugated eigen-states of elliptical polarization…….……25
4.4. An opportunity for Gaussian apodization by a multi-prism expander……28

5. Conclusive remarks……..31

6. Acknowledgnents……..…....31

7. References ……31

ABSTRACT

The most significant problems of determining the dynamic range of new acousto-optical spectrometers and processors for astrophysical applications are under discussion. In so doing, two factors governing the dynamic range of these acousto-optical systems are chosen for the investigations. At first, the influence of the acoustic attenuation along large-aperture acousto-optical cells on the desired levels of lobes in a focal plane of the integrating lens as analyzed, and then potential capabilities of exploiting the incident light beam apodization for increasing the dynamic range of those acousto-optical systems are considered theoretically and within preliminary experiments.

Key words: acousto-optics, linear acoustic waves, linear acoustic attenuation, dynamic range of optical system, crystalline acousto-optical cell, Gaussian profile, light beam apodization.

1. INTRODUCTION

Here, we consider one of the most important problems related to optimizing the performance data of new acousto-optical spectrometers for the analysis of both optical and radio-wave astronomical signals as well as to improving the capabilities of the triple product processors for astrophysical applications. The main attention is paid to estimating two factors governing the dynamic range of these acousto-optical systems. At the beginning, we determine the influence of the acoustic attenuation along large-aperture acousto-optical cells on the expected levels of lobes in a focal plane of the integrating lens and then describe capabilities of the incident light beam apodization for increasing the dynamic range of above-enumerated acousto-optical systems. In particular, these studies lie in a line with the program of the developing metrological equipment for Mexican Large Millimeter Telescope. At first, the Akhieser mechanism responsible for linear attenuation of both longitudinal and shear elastic waves in isotropic and anisotropic solids is analyzed in details. Similar analysis can be directly applied to crystalline materials as well in all the cases of passing elastic wave along the acoustic axis in crystals. After that, we estimate the influence of the acoustic attenuation along large-aperture acousto-optical cells operating in a one-phonon Bragg light scattering regime. Finally, the combined effect of the acoustic attenuation and the incident light beam apodization is studied from the viewpoints of optimizing both the levels of side lobes and the minima inherent in light distribution of an individual resolvable spot in a focal plane of the integrating lens i.e., consequently, estimating potential limitations of the dynamic range.

It is well known that an appropriate apodization of the light beam within acousto-optical data processing makes it possible to increase the potential dynamic range of a system up to $\mathbf{40\ dB}$ and more. Customary, the Gaussian apodization is used when a light beam incidents on a rectangular uniform operative aperture of acousto-optical cell. However, modern acousto-optics exploits often rather high-frequency radio-wave signals in a view of increasing the frequency bandwidth by itself or/and growing the time-bandwidth product inherent in a cell. Anyway, similar acousto-optical cells operate with such frequencies that acoustic losses become already pronounced, so that the effect of these losses along an aperture of a cell has to be taken into account. Typically, acceptable level of the acoustic losses accounts about $\mathbf{3-6\ dB}$ per cell's aperture. By this it means that the expected non-uniformity of distributing the acoustic energy is now not negligible. To obtain really optimized profile of the incident light beam apodization the expected influence of acoustic losses ought to be analyzed and estimated. In connection with aforementioned non-uniformity or asymmetry, one can propose exploiting a quasi-Gaussian profile of the incident light beam reasonably shifted relative to the center of an aperture of the acousto-optical cell with appreciable acoustic losses. The corresponding theoretical estimations are performed as well.

2. LINEAR ACOUSTIC WAVES AND THEIR LINEAR ATTENUATION

2.1. LINEAR ELASTIC WAVES IN SOLIDS

Infinite isotropic solids as well as crystals, oriented along some symmetry axis, allow existing the elastic waves of two types. The first type, longitudinal elastic wave, is characterized by displacements of individual particles along the direction of propagation for a wave. The second one, shear elastic wave, exhibits the displacement of particles in a plane, which is orthogonal to the direction of wave's propagation. In the most general case of anisotropic media, elastic waves can be neither longitudinal or shear in behavior, but here we will consider only specific directions in such media, namely, so-called acoustic axes whose physical properties are quite similar to the properties of isotropic media and allow their description in terms perfectly analogous to the description of elastic waves in isotropic media. Elastic motion in solids can be explained in terms of tensors characterizing the stresses and the deformations [2.1]. Components σ_{ij} of the stresses tensor σ determine forces acting on an elemental area of a solid. With the assumed absence of volumetric momenta, the stresses tensor can be considered as a symmetric one, providing the symmetry $\sigma_{ij} = \sigma_{ji}$. The deformations tensor ε is governed by a pair of the coordinates $\vec{x}(x_i)$ and $\vec{x}'(x_i)$ for the same point before and after deformation, which lead to the displacement vector $\vec{u}(x_i) = \vec{x}'(x_i) - \vec{x}(x_i)$. Generally, the displacement vector can include three contributions, namely, translations and rotations of a body as whole and local deformations. However, the relations between elastic waves and lattice properties need only the last contribution. That is why we will associate the displacement vector $\vec{u}(x_i)$ with local deformations. Comparing the distances between a pair of points before and after deformation and using the relation $\vec{x}' = \vec{u}(x_i) + \vec{x}(x_i)$, one can write $dx'_k = dx_k + \frac{\partial u_k}{\partial x_j} dx_j$, $\delta x'_k = \delta x_k + \frac{\partial u_k}{\partial x_i} \delta x_i$ and consider the following quadratic form $\delta x'_k\, dx'_k - dx_k\, \delta x_k = 2\varepsilon_{mn}\, dx_m\, \delta x_n$, where

$$\varepsilon_{mn} = \frac{1}{2}\left(\frac{\partial u_n}{\partial x_m} + \frac{\partial u_m}{\partial x_n} + \frac{\partial u_l}{\partial x_m}\frac{\partial u_l}{\partial x_n} \right) \tag{2.1}$$

are the components of the deformations tensor ε. It is seen from Eq.(2.1) that the tensor ε is symmetric in behavior, because $\varepsilon_{mn} = \varepsilon_{nm}$. For the further analysis we restrict ourselves by linear approximation and omit the last cross-term in Eq.(2.1). Relative variations of a volume connected with deformations are determined by a value of $Tr\,(\varepsilon_{mn})$. Rewriting Eq.(2.1) as $\varepsilon_{mn} = (\varepsilon_{mn} - \frac{1}{3}\delta_{mn}\varepsilon_{ll}) + \frac{1}{3}\delta_{mn}\varepsilon_{ll}$, one can find that an arbitrary deformation can be represented as a sum of a simple shear and an all-directional compression. Actually, the first summand does not lead to varying the volume, because $Tr\,(\varepsilon_{mn} - \frac{1}{3}\delta_{mn}\varepsilon_{ll}) = 0$; it describes a shear deformation. The second summand $\delta_{mn}\varepsilon_{ll}/3$ characterizes a volumetric deformation.

Now, a matter equation should be taken into account. Such an equation introduces the functional connection between the stresses and the deformations in a solid. In the chosen above linear approximation, the most general form of similar equation is given by $\sigma_{ij} = c_{ijmn}\varepsilon_{mn}$, where c_{ijmn} are the elastic moduli whose number equals to 81. The requirement of symmetry for the tensors σ and ε together with the fact of existing the elastic potential reduce the number of elastic moduli to 21, which is a maximum number for crystals. In isotropic medium, the elastic moduli are independent on directions of the coordinate axes, so that

one arrives at a set of only 3 different non-zero moduli: $\lambda = \mathbf{c_{12}} = \mathbf{c_{13}} = \mathbf{c_{23}}$, $\mu = \mathbf{c_{44}} = \mathbf{c_{55}} = \mathbf{c_{66}}$, and $\lambda + \mathbf{2}\mu = \mathbf{c_{11}} = \mathbf{c_{22}} = \mathbf{c_{33}}$. As a result, the matter equation in isotropic medium can be written as $\sigma_{\mathbf{ij}} = \lambda\, \delta_{\mathbf{ij}} \varepsilon_{\mathbf{kk}} + \mathbf{2}\mu\, \varepsilon_{\mathbf{ij}}$.

To find the elastic motion equations one has to estimate forces acting in a medium. The full force $\vec{\mathbf{F}}$ acting on a volume $\mathbf{v}$ can be considered as a sum of all the forces acting on elemental volumes $\mathbf{dv}$ of a medium. The components $\mathbf{F_i}$ of the force $\vec{\mathbf{F}}$ can be explained through divergence of the stresses tensor as

$$\int_{\mathbf{v}} \mathbf{F_i}\, \mathbf{dv} = \int_{\mathbf{v}} \frac{\partial \sigma_{\mathbf{ij}}}{\partial \mathbf{x_j}} \mathbf{dv} = \oint \sigma_{\mathbf{ij}}\, \mathbf{n_j}\, \mathbf{ds}\,, \tag{2.2}$$

where $\mathbf{ds}$ is an elemental area of a surface, and $\mathbf{n_j}$ is the component of unit normal to an elemental area $\mathbf{ds}$ of that surface. Let us apply the second Newton's law, i.e. equate the force component $\mathbf{F_i}$ to the corresponding component of the acceleration multiplied by the matter density ρ of a medium, and write

$$\frac{\partial \sigma_{\mathbf{ij}}}{\partial \mathbf{x_j}} = \rho\, \frac{\partial^{\mathbf{2}} \mathbf{u_i}}{\partial \mathbf{t^2}}\ . \tag{2.3}$$

Using the matter equation for isotropic medium and the linearized form of Eq.(2.1), one can rewrite Eq.(2.3) as:

$$\frac{\partial \sigma_{\mathbf{ij}}}{\partial \mathbf{x_j}} = \mu\, \frac{\partial^{\mathbf{2}} \mathbf{u_i}}{\partial \mathbf{x_j^2}} + (\lambda + \mu)\, \frac{\partial^{\mathbf{2}} \mathbf{u_k}}{\partial \mathbf{x_k}\, \partial \mathbf{x_i}} = \rho\, \frac{\partial^{\mathbf{2}} \mathbf{u_i}}{\partial \mathbf{t^2}}\ . \tag{2.4}$$

Now, we introduce the factors $\mathbf{V_L} = \sqrt{(\lambda + \mathbf{2}\mu)/\rho}$ and $\mathbf{V_S} = \sqrt{\mu/\rho}$, then take into account the vector relations $\frac{\partial \mathbf{u_k}}{\partial \mathbf{x_k}} = \mathbf{div}\, \vec{\mathbf{u}}$ and $\frac{\partial^{\mathbf{2}} \mathbf{u_i}}{\partial \mathbf{x_j^2}} = \nabla^{\mathbf{2}}\, \vec{\mathbf{u}}$, and convert Eq.(2.4) into

$$\mathbf{V_L^2}\ \mathbf{grad}\,(\mathbf{div}\, \vec{\mathbf{u}}) - \mathbf{V_S^2}\ \mathbf{rot}\ \mathbf{rot}\, \vec{\mathbf{u}} = \frac{\partial^{\mathbf{2}} \vec{\mathbf{u}}}{\partial \mathbf{t^2}}\,. \tag{2.5}$$

The vector $\vec{\mathbf{u}}$ can be always represented as the sum $\vec{\mathbf{u}} = \vec{\mathbf{u}}_{\mathbf{L}} + \vec{\mathbf{u}}_{\mathbf{S}}$, where $\vec{\mathbf{u}}_{\mathbf{L}} = \mathbf{grad}\, \psi$ and $\vec{\mathbf{u}}_{\mathbf{S}} = \mathbf{rot}\, \vec{\mathbf{A}}$. Due to $\mathbf{rot}\, \vec{\mathbf{u}}_{\mathbf{L}} = \mathbf{rot}\ \mathbf{grad}\, \psi \equiv \mathbf{0}$ and $\mathbf{div}\, \vec{\mathbf{u}}_{\mathbf{S}} = \mathbf{div}\ \mathbf{rot}\, \vec{\mathbf{A}} \equiv \mathbf{0}$, one can exploit the operator equality $\nabla^{\mathbf{2}} = \mathbf{grad}\ \mathbf{div} - \mathbf{rot}\ \mathbf{rot}$ and divide Eq.(5) into a pair of the following independent evolution equations

$$\text{a)}\ \ \nabla^{\mathbf{2}}\, \vec{\mathbf{u}}_{\mathbf{L}} = \mathbf{V_L^{-2}}\, \frac{\partial^{\mathbf{2}} \vec{\mathbf{u}}_{\mathbf{L}}}{\partial\, \mathbf{t^2}}\ ,\quad \mathbf{rot}\, \vec{\mathbf{u}}_{\mathbf{L}} = \mathbf{0}\ ; \qquad \text{b)}\ \ \nabla^{\mathbf{2}}\, \vec{\mathbf{u}}_{\mathbf{S}} = \mathbf{V_S^{-2}}\, \frac{\partial^{\mathbf{2}} \vec{\mathbf{u}}_{\mathbf{S}}}{\partial\, \mathbf{t^2}}\ ,\quad \mathbf{div}\, \vec{\mathbf{u}}_{\mathbf{S}} = \mathbf{0} \tag{2.6}$$

for the displacements $\vec{\mathbf{u}}_{\mathbf{L}}$ and $\vec{\mathbf{u}}_{\mathbf{S}}$ of the longitudinal and shear elastic waves, respectively. Here, the factors $\mathbf{V_L}$ and $\mathbf{V_S}$ play parts of the corresponding phase velocities of propagation. Thus, one can see that both longitudinal and shear elastic waves are governed by quite similar evolution equation, the wave equations, so that hereafter the index of wave's type could be omitted.

2.2. LINEAR ACOUSTIC ATTENUATION

One of the most important parameters in the theory of acoustic attenuation represents the ratio of the acoustic wavelength Λ to the averaged mean free pass $\mathbf{l_F}$ of thermal phonons in a crystal. Calling τ the averaged temporal interval between collision of thermal phonons and Ω the frequency of elastic wave, one can consider two limiting cases. If $\Lambda << \mathbf{l_F}$ and, consequently, $\Omega\tau >> \mathbf{1}$, this is meant that the attenuation of acoustic phonons is conditioned by their collisions with a lattice whose phonons are in a state of thermal equilibrium. This case was considered by L.Landau and G.Rumer [2.2], and G.L.Slonimsky [2.3]; usually, it corresponds to the low temperature area, i.e. to the absolute temperature range of $\mathbf{T < 50^0\,K}$ when the frequency of elastic wave is about $\mathbf{1\,GHz}$. The opposite case of $\Omega\tau << \mathbf{1}$ makes it possible to consider thermal phonons as particles propagating in a slowly varying potential field, caused by the elastic wave. In fact, it means that the coherent elastic wave destroys an equilibrium distribution of thermal phonons, which become to be not governed by the equilibrium Planck distribution. Growing the entropy, needed for recovering the thermal equilibrium of these phonons, leads to attenuation of elastic energy. For the majority of crystals, this mechanism, revealed and described by A.Akhieser [2.4], can be observed at temperatures $\mathbf{T > 50^0\,K}$ and frequencies up to $\mathbf{1\,GHz}$. The last case is very close to typical acousto-optic experimental situations, so that it is really worthwhile to apply just the Akhieser's mechanism to characterization of the attenuating elastic waves in acousto-optical crystals.

The interaction between the coherent elastic wave and the phonons of heat modes leads to increasing the number of phonons in some heat modes up to the value $\mathbf{n}$ [2.5], which differs on the equilibrium value $\bar{\mathbf{n}}$. Let us follow the behavior of an individual mode (index 1) inherent in the coherent elastic wave, which includes $\mathbf{n_1^0}$ coherent phonons before the interaction. All the other modes, related to heat phonons, are in thermodynamic equilibrium with each other. After the temporal interval $\mathbf{t}$ the probability $\mathbf{W^- t}$ appears that the number $\mathbf{n_1^0}$ will be decreased by unity due to the corresponding nonlinear elastic interactions in a system, i.e. due to colliding one of the coherent phonons with one of the heat ones. Figure 2.1 illustrates similar process when the number of coherent phonons becomes to be $\mathbf{n_1 = n_1^0 - 1}$, while the numbers of heat mode phonons (indices 2 and 3) are now $\mathbf{n_2 = \bar{n}_2 - 1}$ and $\mathbf{n_3 = \bar{n}_3 + 1}$. At the same time, another phonon processes will aspire to recover that equilibrium. In particular, similar probability $\mathbf{W^+ t}$ exists that the

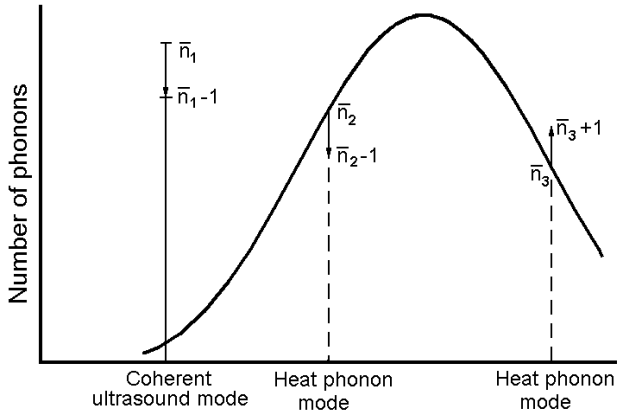

Figure 2.1. Schematic representation for the phonon spectrum and the modes under consideration

number $\mathbf{n_1}$ will increase by one phonon, so that $\mathbf{n_1 = n_1^0 + 1}$. The difference of these two probabilities $\mathbf{W^+ t - W^- t = n_1 - \bar{n}_1}$ represents the probability of varying the number $\mathbf{n_1}$ from the equilibrium value $\mathbf{\bar{n}_1}$. The velocity of such varying the number $\mathbf{n_1}$ can be estimated by

$$\text{a)}\ \frac{\partial(\mathbf{n_1 - \bar{n}_1})}{\partial \mathbf{t}} = \mathbf{W^+ - W^-} \qquad \text{or} \qquad \text{b)}\ \frac{\partial \mathbf{n_1}}{\partial \mathbf{t}} = \mathbf{W^+ - W^-}, \tag{2.7}$$

because the equilibrium value $\mathbf{\bar{n}_1}$ does not depend on time. It follows from Eq.(2.7a) that $\mathbf{W^+ - W^- = (W_0^+ - W_0^-)(n_1 - \bar{n}_1)}$. Introducing $\mathbf{-1/\tau = (W_0^+ - W_0^-)}$, one can write

$$\text{a)}\ \frac{\mathbf{1}}{\tau} = \frac{\mathbf{-1}}{\mathbf{(n_1 - \bar{n}_1)}} \frac{\partial(\mathbf{n_1 - \bar{n}_1})}{\partial \mathbf{t}} \quad \text{or} \quad \text{b)}\ \frac{\mathbf{1}}{\tau} = \frac{\mathbf{-1}}{\hbar\omega\,\mathbf{(n_1 - \bar{n}_1)}} \frac{\partial\,[\hbar\omega\,(\mathbf{n_1 - \bar{n}_1})]}{\partial \mathbf{t}} = -\frac{\mathbf{1}}{\mathbf{W}} \frac{\partial \mathbf{W}}{\partial \mathbf{t}}, \tag{2.8}$$

where $\mathbf{W}$ is the energy absorbed by the heat phonon assembly or lost by the coherent elastic wave. Consequently, one can write that $\mathbf{W = W_0\ exp(-t/\tau)}$, where τ has a meaning of the relaxation time. Of course, the last relation is phenomenological in behavior and it can be applied to practically an arbitrary system with losses.

The energy loss of the coherent elastic wave can be characterized by the logarithmic decrement δ describing the attenuation. For a system performing free harmonic oscillations with a small attenuation, such a decrement can be determined as $\mathbf{\delta = W/(2E)}$, where $\mathbf{W}$ can be considered as energy loss for one period of oscillations and $\mathbf{E}$ is the total energy of oscillations stored for one period in a crystalline sample. Consequently, one can write

$$\delta = \frac{\mathbf{1}}{\mathbf{2W}\nu_\mathbf{R}} \frac{\partial \mathbf{W}}{\partial \mathbf{t}}, \tag{2.9}$$

where $\nu_\mathbf{R}$ is the resonant frequency inherent in this oscillating system with losses. Here, the logarithmic decrement δ is measured in nepers. It is seen from Eqs.(2.2) and (2.3) that $\mathbf{2}\nu_\mathbf{R}\,\tau\,\delta = \mathbf{1}$. Then, one can write the following standard relations for the coefficient α of linear losses related to the coherent elastic mode

$$\begin{aligned} &\text{a)}\ \alpha\,\mathbf{(dB/\mu s)} = \mathbf{8.68 \cdot 10^{-6}}\ \nu_\mathbf{R}\ \delta\mathbf{(Np)} = \mathbf{4.34 \cdot 10^{-6}}\ \tau^{\mathbf{-1}}, \\ &\text{b)}\ \alpha\,\mathbf{(dB/cm)} = \mathbf{V^{-1}}\ \alpha\,\mathbf{(dB/\mu s) \cdot 10^6} = \mathbf{4.34}\ \tau^{\mathbf{-1}}\,\mathbf{V^{-1}}, \end{aligned} \tag{2.10}$$

where $\mathbf{V}$ is the velocity of the chosen coherent elastic mode. Now, we have to estimate the coefficient α of linear losses for elastic waves whose frequency does not exceed $\mathbf{1\,GHz}$.

2.3. THE AKHIESER'S MECHANISM OF LOSSES FOR THE COHERENT ELASTIC WAVE

The presence of a coherent elastic mode in solid state leads to varying elastic properties of a medium and, consequently, the frequency of Debye's phonons. For small distortions, the classic theory of elasticity is true, so that the variation of phonon frequency can be extended into a series in terms of powers for the deformations $\varepsilon_{\mathbf{ij}}$ and the rotations $\omega_\mathbf{i}$. In the first approximation relatively to these tensors, one can write

$$\omega_j(\vec{q}) = \omega_j^0(\vec{q})\left[1 + \gamma_{ij}(\vec{q})\varepsilon_{ij} + \gamma_i'(\vec{q})\omega_i\right], \tag{2.11}$$

where $\omega_j^0(\vec{q})$ is the phonon frequency in the absence of the coherent elastic wave, $\gamma_{ij}(\vec{q})$ are the Gruneisen factors. Broadly speaking, the factors γ_{ij} depend on $\vec{q}$. However, if the dispersion is negligibly small in a system, the factors γ_{ij} depend only on the direction of the wave vector $\vec{q}$ rather than its modulus. The coefficient α of linear losses for elastic waves is determined in terms of the quantity of heat scattered inside unit of volume per unit of time. In other words, one has to calculate the velocity of varying the entropy S of phonon gas multiplied by the absolute temperature T. The entropy S of phonon is given by [2.6]

$$S = K\sum_{\vec{q},j}\left\{[n_j(\vec{q})+1]\ln[n_j(\vec{q})+1] - n_j(\vec{q})\ln[n_j(\vec{q})]\right\}, \tag{2.12}$$

where K is the Boltzmann constant. Direct differentiation gives the following expression for the dissipative function

$$T\frac{dS}{dt} = KT\sum_{\vec{q},j}\frac{dn_j(\vec{q})}{dt}\ln\left[\frac{n_j(\vec{q})+1}{n_j(\vec{q})}\right]. \tag{2.13}$$

Restricting ourselves by three-phonon processes only, let us consider phonon mode with the wave vector $\vec{q}_1$. The velocity of varying $n(\vec{q}_1)$ due to the presence of coherent elastic wave under stationary conditions can be estimated via equating to zero a sum of the two temporal derivatives

$$\left[\frac{dn(\vec{q}_1)}{dt}\right]_{collisions} + \left[\frac{dn(\vec{q}_1)}{dt}\right]_{ultrasound} = 0. \tag{2.14}$$

In the assumption that $n(\vec{q}) = n^0(\vec{q}) + \Delta n(\vec{q})$, we exploit the results of a three-phonon theory keeping only the contributions being linear in behavior relatively to the variations $\Delta n(\vec{q})$. In so doing, one can obtain

$$\left[\frac{dn(\vec{q}_1)}{dt}\right]_{collisions} = \frac{-\pi\hbar}{4N}\sum_{\vec{q}_2,\vec{q}_3}|M|^2\left\{2\sinh\frac{\hbar\omega(\vec{q}_1)}{2KT}\sinh\frac{\hbar\omega(\vec{q}_2)}{2KT}\sinh\frac{\hbar\omega(\vec{q}_3)}{2KT}\right\}^{-1}\times \tag{2.15}$$

$$\left\{\left[-\Delta n(\vec{q}_1)\sinh^2\frac{\hbar\omega(\vec{q}_1)}{2KT} + \Delta n(-\vec{q}_2)\sinh^2\frac{\hbar\omega(\vec{q}_2)}{2KT} + \Delta n(-\vec{q}_3)\sinh^2\frac{\hbar\omega(\vec{q}_3)}{2KT}\right]\delta[\omega(\vec{q}_1)-\omega(\vec{q}_2)-\omega(\vec{q}_3)] + \right.$$

$$\left[-\Delta n(\vec{q}_1)\sinh^2\frac{\hbar\omega(\vec{q}_1)}{2KT} + \Delta n(-\vec{q}_2)\sinh^2\frac{\hbar\omega(\vec{q}_2)}{2KT} - \Delta n(-\vec{q}_3)\sinh^2\frac{\hbar\omega(\vec{q}_3)}{2KT}\right]\delta[\omega(\vec{q}_1)-\omega(\vec{q}_2)+\omega(\vec{q}_3)] +$$

$$\left.\left[-\Delta n(\vec{q}_1)\sinh^2\frac{\hbar\omega(\vec{q}_1)}{2KT} - \Delta n(-\vec{q}_2)\sinh^2\frac{\hbar\omega(\vec{q}_2)}{2KT} + \Delta n(-\vec{q}_3)\sinh^2\frac{\hbar\omega(\vec{q}_3)}{2KT}\right]\delta[\omega(\vec{q}_1)+\omega(\vec{q}_2)-\omega(\vec{q}_3)]\right\}$$

.

Here, $|M|^2$ is the matrix element of the corresponding phonon transition and N is the number of particles in the model under consideration. Then, rather small variation $\Delta n(\vec{q})$ can be expressed as

$\Delta \mathbf{n}(\vec{\mathbf{q}}) = -\phi(\vec{\mathbf{q}})\,[\partial \mathbf{n}^{\mathbf{0}}(\vec{\mathbf{q}})/\partial \hbar\omega(\vec{\mathbf{q}})]$, where $\phi(\vec{\mathbf{q}})$ is unknown value to be found. Using the last formula, one can immediately write

$$\Delta \mathbf{n}(\vec{\mathbf{q}}) = \mathbf{n}^{\mathbf{0}}(\vec{\mathbf{q}}) + \frac{\phi(\vec{\mathbf{q}})}{\mathbf{KT}}\,\mathbf{n}^{\mathbf{0}}(\vec{\mathbf{q}})\left[\mathbf{n}^{\mathbf{0}}(\vec{\mathbf{q}}) + \mathbf{1}\right] = \mathbf{n}^{\mathbf{0}}(\vec{\mathbf{q}}) + \frac{\phi(\vec{\mathbf{q}})}{\mathbf{KT}}\,\mathbf{sinh}^{-2}\frac{\hbar\omega(\vec{\mathbf{q}})}{\mathbf{2KT}}. \tag{2.16}$$

That is why Eq.(2.15) can be rewritten as

$$\left[\frac{\mathbf{dn}(\vec{\mathbf{q}}_1)}{\mathbf{dt}}\right]_{\mathbf{collisions}} = \frac{-\pi\hbar}{\mathbf{32N}} \sum_{\vec{\mathbf{q}}_2,\,\vec{\mathbf{q}}_3} |\mathbf{M}|^2 \left\{\mathbf{KT}\sinh\frac{\hbar\omega(\vec{\mathbf{q}}_1)}{\mathbf{2KT}}\,\sinh\frac{\hbar\omega(\vec{\mathbf{q}}_2)}{\mathbf{2KT}}\,\sinh\frac{\hbar\omega(\vec{\mathbf{q}}_3)}{\mathbf{2KT}}\right\}^{-1} \times$$

$$\left\{\left[-\phi(\vec{\mathbf{q}}_1)+\phi(-\vec{\mathbf{q}}_2)+\phi(-\vec{\mathbf{q}}_3)\right]\,\delta[\omega(\vec{\mathbf{q}}_1)-\omega(\vec{\mathbf{q}}_2)-\omega(\vec{\mathbf{q}}_3)]+\right. \tag{2.17}$$

$$\left[-\phi(\vec{\mathbf{q}}_1)+\phi(-\vec{\mathbf{q}}_2)-\phi(-\vec{\mathbf{q}}_3)\right]\,\delta[\omega(\vec{\mathbf{q}}_1)-\omega(\vec{\mathbf{q}}_2)+\omega(\vec{\mathbf{q}}_3)]+$$

$$\left.\left[-\phi(\vec{\mathbf{q}}_1)-\phi(-\vec{\mathbf{q}}_2)+\phi(-\vec{\mathbf{q}}_3)\right]\,\delta[\omega(\vec{\mathbf{q}}_1)+\omega(\vec{\mathbf{q}}_2)-\omega(\vec{\mathbf{q}}_3)]\right\}.$$

Coming back to Eq.(2.13) and substituting $\mathbf{n}(\vec{\mathbf{q}})$, one can obtain

$$\mathbf{T}\frac{\mathbf{dS}}{\mathbf{dt}} = \mathbf{KT}\sum_{\vec{\mathbf{q}}_1}\frac{\mathbf{dn}(\vec{\mathbf{q}}_1)}{\mathbf{dt}}\,\ln\left[\frac{\mathbf{n}^{\mathbf{0}}(\vec{\mathbf{q}}_1)+1}{\mathbf{n}^{\mathbf{0}}(\vec{\mathbf{q}}_1)}\right] + \mathbf{KT}\sum_{\vec{\mathbf{q}}_1}\frac{\mathbf{dn}(\vec{\mathbf{q}}_1)}{\mathbf{dt}}\,\ln\left[1-\frac{\phi(\vec{\mathbf{q}})}{\mathbf{KT}}\right]. \tag{2.18}$$

Using Eq.(2.14), one can replace $\mathbf{dn}(\vec{\mathbf{q}}_1)/\mathbf{dt}$ by $-[\mathbf{dn}(\vec{\mathbf{q}}_1)/\mathbf{dt}]_{\mathbf{collisions}}$ from Eq.(2.17) in Eq.(2.18). In this case, the first summand of Eq.(2.18) equals zero, while the second summand in the approximation of $\ln(1-\mathbf{x}) \approx \mathbf{x}$ for small $\mathbf{x}$ with an accuracy of the second order terms in respect to ϕ gives

$$\mathbf{T}\frac{\mathbf{dS}}{\mathbf{dt}} = \frac{-\pi\hbar}{\mathbf{32N}} \sum_{\vec{\mathbf{q}}_1,\,\vec{\mathbf{q}}_2,\,\vec{\mathbf{q}}_3} |\mathbf{M}|^2 \left\{\mathbf{KT}\sinh\frac{\hbar\omega(\vec{\mathbf{q}}_1)}{\mathbf{2KT}}\,\sinh\frac{\hbar\omega(\vec{\mathbf{q}}_2)}{\mathbf{2KT}}\,\sinh\frac{\hbar\omega(\vec{\mathbf{q}}_3)}{\mathbf{2KT}}\right\}^{-1} \times$$

$$\left[\phi(\vec{\mathbf{q}}_1)-\phi(-\vec{\mathbf{q}}_2)-\phi(-\vec{\mathbf{q}}_3)\right]^2\;\;\delta[\omega(\vec{\mathbf{q}}_1)-\omega(\vec{\mathbf{q}}_2)-\omega(\vec{\mathbf{q}}_3)]\,. \tag{2.19}$$

If the dissipative function, i.e. the left hand side of Eq.(2.19), is known, one can find the factor of elastic losses. In so doing, let us consider at first a contribution of the thermo-elastic effect and write

$$\text{a)}\;\;\frac{\mathbf{dS}}{\mathbf{dt}} = \kappa\int \mathbf{T}^{-2}\,(\mathbf{grad}\,\mathbf{T})^2\,\mathbf{dV}\,, \qquad \text{b)}\;\;\mathbf{grad}\,\mathbf{T} = -\frac{\mathbf{3T}\beta_{\mathbf{0}}}{\mathbf{C_V}}\left[\mathbf{c_{11}} - \frac{\mathbf{2}}{\mathbf{3}}\left(\mathbf{c_{11}}-\mathbf{c_{12}}\right)\right]\varepsilon_{\mathbf{ii}}\,, \tag{2.20}$$

where κ is the adiabatic thermal conductivity of a medium, $\mathbf{C_V}$ is the specific heat capacity at the constant volume, $\beta_{\mathbf{0}}$ is the adiabatic expansion factor, $\mathbf{c_{kl}}$ are the corresponding elastic moduli, and $\varepsilon_{\mathbf{ii}}$ is the diagonal component of the deformation tensor. It follows from Eq.(2.20b) that $\mathbf{grad}\,\mathbf{T} = \mathbf{0}$ for the shear elastic waves, so that thermo-elasticity cannot contribute in the attenuation of shear waves. When temperature $\mathbf{T}$ depends on the point of estimation inside a medium only slightly, one can take the term $\mathbf{T}^{-2}$ out of the integral in Eq.(2.20a), so that the velocity of energy dissipation due to thermo-elasticity can be estimated by

$$\frac{dE_D}{dt} = -\kappa T^{-1} \int (\mathrm{grad} T)^2 \, dV \ . \qquad (2.21)$$

For example, if the longitudinal elastic wave (see the index L) is passing along the $z-$axes, so that $u_x = u_y = 0$ and $u_z = u_0 \exp[i(q_L z - \omega_L t)]$, one can calculate a pair of the period average values as

$$\text{a)} \ \frac{1}{V_L}\left\langle \frac{dE_D}{dt} \right\rangle = -\frac{\kappa}{2T}\left(\frac{3T\beta_0}{C_V}\right)^2 \left[c_{11} - \frac{2}{3}(c_{11} - c_{12}) \right]^2 u_0^2 q_L^4 , \qquad \text{b)} \ \frac{1}{V_L}\langle E \rangle = \frac{1}{2} u_0^2 \rho \, \omega_L^2 , \qquad (2.22)$$

where the time average energy E in solid state is equal to the twiced kinetic energy. Thus, the factor of elastic losses represents a ratio of the average velocity of energy dissipation to the twiced average energy flow, i.e.

$$\alpha = -\frac{1}{2V_L\langle E \rangle}\left\langle \frac{dE_D}{dt} \right\rangle = \frac{\kappa}{2T}\left(\frac{3T\beta_0}{C_V}\right)^2 \left[c_{11} - \frac{2}{3}(c_{11} - c_{12}) \right]^2 \frac{\omega_L^2}{V_L^5} = \frac{\kappa \xi^2 T \omega_L^2}{\rho V_L^5} \ , \qquad (2.23)$$

where ξ is the effective Gruneisen constant and ρ is the matter density. Due to $\kappa \sim T^{-1}$, the coefficient α of linear elastic losses is independent on the temperature in agreement with the experimental data at room temperature, but α has a square-law dependence on the cyclic ω_L frequency of the longitudinal elastic wave.

The shear elastic wave attenuation can be estimated through the consideration of viscosity. In this case, the dissipative function Φ includes time derivatives of the deformation tensor $\Phi = (1/2)\eta_{ijkm}(d\varepsilon_{ij}/dt)(d\varepsilon_{km}/dt)$, where η is the tensor of viscosity. This tensor consists of only two coefficients η_1 and η_2 in isotropic medium, so that the dissipative function Φ takes the form

$$\Phi = \eta_1 \left(\frac{d\varepsilon_{ij}}{dt} - \frac{\delta_{ij}}{3}\frac{d\varepsilon_{kk}}{dt} \right)^2 + \frac{1}{2}\eta_2 \left(\frac{d\varepsilon_{kk}}{dt} \right)^2 \ . \qquad (2.24)$$

The velocity of energy dissipation due to viscosity can be estimated by

$$\frac{dE_D}{dt} = \int \left\{ -2\eta_1 \left(\frac{d\varepsilon_{ij}}{dt} - \frac{\delta_{ij}}{3}\frac{d\varepsilon_{kk}}{dt} \right)^2 - \eta_2 \left(\frac{d\varepsilon_{kk}}{dt} \right)^2 \right\} dV \ . \qquad (2.25)$$

In contrast with the thermo-elastic effect considered above, Eq.(2.25) includes both diagonal and non-diagonal components of the deformation tensor. That is why using the approach, presented previously by Eqs.(2.22) and (2.23) for the thermo-elastic effect, one can determine the factors α of elastic losses, conditioned by the viscosity for both longitudinal and shear elastic waves (see the indices L and T, respectively) as

$$\text{a)} \ \alpha_L = \left(\frac{4}{3}\eta_1 + \eta_2 \right) \frac{\omega_L^2}{2\rho V_L^3} \ , \qquad \text{b)} \ \alpha_T = \frac{\eta_1 \omega_T^2}{2\rho V_T^3} \ . \qquad (2.26)$$

It is seen from Eq.(2.26) that as before the factor α has a square-law dependence on the frequency of elastic wave.

2.4. EFFECT OF LINEAR ACOUSTIC ATTENUATION ALONG A DISTANCE OF ELASTIC WAVE PROPAGATION

The effect of acoustic attenuation can be considered using the Hook low, which includes the tensor η of viscosity:

$$\sigma_{ij} = c_{ijkl}\,\varepsilon_{ij} + \eta_{ijkl}\frac{\partial \varepsilon_{kl}}{\partial t} \ . \tag{2.27}$$

Here, σ and c are the tensors of stresses and elastic modules as before. The propagation of high-frequency elastic (acoustic) waves with the amplitude u_k and the cyclic frequency Ω is described by the Christoffel equation

$$(\Lambda_{ik} + i\Omega\, D_{ik} - \rho V^2 \delta_{ik})\, u_k = 0 \,, \tag{2.28}$$

where $\Lambda_{ik} = c_{ijkl}\, n_j\, n_l$, $D_{ik} = \eta_{ijkl}\, n_j\, n_l$, and n_j is the component of the wave normal unit vector $\vec{n}$. In the case of relatively low acoustic attenuation, Eq.(2.28) allows separating real and imaginary parts as

$$\text{a) } \mathbf{Det}\,|\,\Lambda_{ik} - \rho V^2 \delta_{ik}\,| = 0 \,, \qquad \text{b) } \mathbf{Det}\,|\,D_{ik} - \frac{2\rho V^3 \alpha}{\Omega^2}\cdot\delta_{ik}\,| = 0 \,. \tag{2.29}$$

Thus, Eq.(2.29a) characterizes the phase velocities V of acoustic modes, while Eq.(2.29b) gives the factors of acoustic attenuation α_m for each $m-$ acoustic mode via the relation

$$\alpha_m = \frac{\Omega^2}{2\rho V^3} D_{ik}^m \ , \tag{2.30}$$

where D_{ik}^m is the corresponding eigen-value of the above introduced dissipation tensor D.

The contribution from linear acoustic attenuation to the wave propagation process can be taken into account if Eq.(2.6) will be modified as [2.8]

$$\nabla^2 \vec{u} - V^{-2}\frac{\partial^2 \vec{u}}{\partial t^2} + b\,\frac{\partial}{\partial t}\nabla^2 \vec{u} = 0 \ , \tag{2.31}$$

where b is the factor of acoustic losses. The solution to Eq.(2.31) can be found in the form of $\vec{u}(\vec{r},t) = \vec{m}\,A(x)\exp(-i\Omega t)$. Substituting this project of solution into Eq.(2.31), we arrive at the Helmholtz equation

$$\frac{d^2 A}{dx^2} + \frac{\Omega^2}{V^2}\left(1 - ib\Omega\right)^{-1} A = 0 \,. \tag{2.32}$$

Substituting a trial solution $\exp(i\kappa x)$ into Eq.(2.32), one can find the characteristic equation $\kappa^2 = \Omega^2 V^2 \left(1 - ib\Omega\right)^{-1}$ whose solutions are

$$\kappa_{1,2} = \Omega V^{-1} \left(1 - i b \Omega\right)^{-1/2} \approx \Omega V^{-1} \left[1 + i (b \Omega / 2)\right] = k + i\alpha , \quad K = \Omega / V , \quad \alpha = b \Omega^2 / (2V) \qquad (2.33)$$

with $(b\Omega/2) << 1$; here $K = \left|\vec{K}\right|$ is the modulus of the wave vector $\vec{K}$ of the elastic wave. Thus, one can express $A(x) = A_1 \exp(i \kappa_1 x) + A_2 \exp(-i \kappa_2 x)$ and then find $\vec{u}(\vec{r}, t)$ as

$$\vec{u}(\vec{r}, t) = \vec{m}\, A_1 \exp(-\alpha x) \exp\left[-i\Omega (t - x/V)\right] + \vec{m}\, A_2 \exp(\alpha x) \exp\left[-i\Omega (t + x/V)\right] . \qquad (2.34)$$

This solution includes the two counter-propagating waves; each of them attenuates exponentially during its passing through a medium in the corresponding direction.

3. ANALYSIS OF THE APODIZATION FOR LIGHT BEAMS BY THE OPTIMIZEDQUASI-GAUSSIAN PROFILES; APPLICATION TO THE ACOUSTO-OPTICAL CELLS WITH APPRECIABLE ACOUSTIC LOSSES

3.1. INTRODUCTIVE REMARKS

At really high acoustic frequencies, the divergence of acoustic beam can be omitted, so that the attenuation will play the dominating role in the expected non-uniformity of distributing the acoustic energy along the cell. Together with this, the effect of acoustic losses is significant due to obvious asymmetry and non-uniformity in distribution of the acoustic energy along optical aperture of a cell. Moreover, the appearing non-uniformity in this distribution is not the same within the frequency bandwidth Δf of a cell. The central frequency f_0 is determined as $\Delta f = p \cdot f_0$. The ratio ν of the highest frequency to the lowest one within a given frequency bandwidth is $\nu = (2+p)/(2-p)$. Usually $p = 1/2$, and one yields $\nu = 5/3$. In its turn, the peak-ratio between two amplitude coefficients of the acoustic losses, corresponding to these pair of boundary frequencies within the bandwidth $\Delta f = f_0/2$, is $\nu^2 \approx 2.78$ due to square-low dependence of the acoustic losses on the frequency. Sometimes, however, a little bit wider frequency bandwidth with $p = 2/3$ and $\Delta f = 2f_0/3$ is exploited, so that in this case $\nu = 2$ and, naturally, $\nu^2 = 4$. Consequently, the expected non-uniformity of distributing the acoustic energy cannot be already omitted. To find sufficiently optimized profile of the incident light beam apodization the expected effect of acoustic attenuation is analyzed and estimated. In a view of aforementioned asymmetry, one can propose exploiting a quasi-Gaussian profile of the incident light beam reasonably shifted relative to the center of an aperture of the acousto-optical cell with appreciable acoustic attenuation.

In signal processing, a window function (or an apodization function) is a mathematical function that is zero-valued outside of some chosen interval. For instance, a function that is constant inside the interval and zero elsewhere is called a rectangular window, which describes the shape of its graphical representation. When another function or a signal is multiplied by a window function, the product is also zero-valued outside the chosen interval. A more general definition of window functions does not require them to be identically zero outside an interval, as long as the product of the window multiplied by its argument is square integrable, that is, that the function goes sufficiently rapidly toward zero. In typical applications, the window functions used are non-negative smooth "bell-shaped" curves, though rectangle, triangle, and other generalized functions are sometimes used. In spectrum analysis, the Fourier transform of the function $\cos(\omega t)$ is zero, except at frequencies $\pm\omega$. However, many other functions do not have convenient closed form transforms, and one might be interested in their spectral content only during a certain period. The Fourier transform can be applied on a finite interval of the function, or in general, the transform is applied to the product of the function and a window function, so that any window (including rectangular) affects the spectrum. Windowing of a simple function, like $\cos(\omega t)$ causes its Fourier transform to develop non-zero values (called spectral leakage) at frequencies other than ω. The leakage tends to be worst (highest) near ω and least at frequencies farthest from ω. If the signal under analysis is composed of two sinusoids of different frequencies, leakage can interfere with the ability to distinguish them spectrally. If their frequencies are dissimilar and one component is weaker, then leakage from the larger component can obscure the weaker's presence. But if the frequencies are similar, leakage can render them unresolvable even when the sinusoids are of equal strength. The rectangular window has excellent resolution characteristics for signals of comparable strength, but it is a poor choice for signals of disparate amplitudes. This characteristic is sometimes described as low-dynamic-range. At the other extreme of dynamic range are the windows with the poorest resolution. These high-dynamic-range low-resolution windows are also poorest in terms of sensitivity; this is, if the input function

contains random noise close to the signal frequency, the response to noise, compared to the sinusoid, will be higher than with a higher-resolution window. In other words, the ability to find weak sinusoids amidst the noise is diminished by a high-dynamic-range window. High-dynamic-range windows are probably most often justified in wideband applications, where the spectrum being analyzed is expected to contain many different signals of various amplitudes. In between the extremes are moderate window, which are commonly used in narrowband applications. In summary, spectral analysis involves a tradeoff between resolving comparable strength signals with similar frequencies and resolving disparate strength signals with dissimilar frequencies. That tradeoff occurs when the window function is chosen. Let us consider a few examples of high- and moderate-resolution windows $\mathbf{W(y)}$ and their Fourier transforms $\mathbf{S(u)}$:

1) The Dirichlet or rectangular window: $\mathbf{W_R = rect\,(y)}$, $\mathbf{S_R = \frac{\sin(\pi u)}{\pi u}}$; (3.1)

2) The cosine window: $\mathbf{W_C = \cos(\pi y)}$, $\mathbf{S_C = \frac{2\cos(\pi u)}{\pi(1-u^2)}}$; (3.2)

3) The "raised cosine" wind $\mathbf{W_H = p + q\cos(2\pi y)}$, $\mathbf{S_H = \frac{\sin(\pi u)}{\pi u}\cdot\left(p + \frac{q u^2}{1-u^2}\right)}$ (3.3)

The last window, see Eqs.(3.3), includes at least two widely used particular cases. The first one is the Hann window, which represents the simplest "raised cosine" window with coefficients $\mathbf{p = q = 0.5}$. In this case the ends of cosine function just touch zero, so that the side lobes roll off at about $\mathbf{18\ dB}$ per octave. The second case is connected with the Hamming window having $\mathbf{p = 0.54}$ and $\mathbf{q = 0.46}$. It was proposed to minimize the maximum (nearest) side lobe, giving it a height of about one-fifth that of the Hann window. Then, one can introduce the profile parameter β and take

4) The Gaussian window: $\mathbf{W_G = \exp(-\beta y^2)}$, $\mathbf{S_G = \sqrt{\frac{\pi}{4\beta}}\exp\left(-\frac{\pi^2 u^2}{\beta}\right)\cdot\left[\mathrm{Erf}\left(\frac{\beta + 2i\pi u}{2\sqrt{\beta}}\right) + \mathrm{Erf}\left(\frac{\beta - 2i\pi u}{2\sqrt{\beta}}\right)\right]}$. (3.4)

The frequency response of a Gaussian is also a Gaussian (it is an eigen-function of the Fourier transform). Since the Gaussian function extends to infinity, it must either be truncated at the ends of the window, or itself windowed with another zero-ended window. Since the logarithm of a Gaussian produces a parabola, this can be used for exact quadratic interpolation in frequency estimation. The comparison of these windows is presented in Fig.3.1. One can see that rectangular window gives the best "frequency resolution", while the others provide better dynamic range. Evidently, the most attractive window looks the Gaussian one, which exhibits a moderate "frequency resolution" and promises rather high dynamic range. Additionally, these characteristics can be varied by an adequate selection of the parameter β.

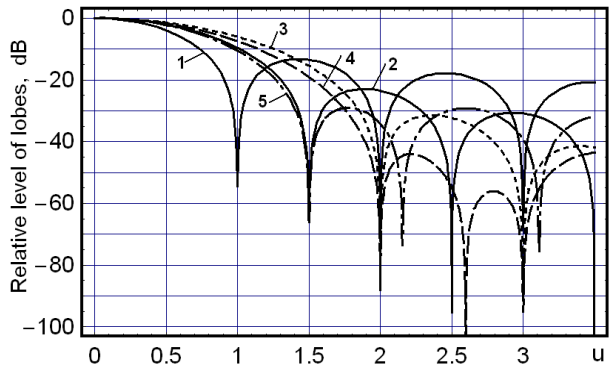

Figure 3.1. The normalized intensity distributions in the Fourier transform plane: 1 is for rectangular, 2 is for the cosine, 3 is for the Hann, 4 is for the Hamming, and 5 is for the Gaussian $(\beta = 6.7)$ windows.

3.2. EFFECT OF ACOUSTIC ATTENUATION ALONG THE APERTURE OF BRAGG ACOUSTO-OPTICAL CELL

The acoustic attenuation in solids has been studied experimentally. It has been found that at room temperature the dominant mechanism of acoustic attenuation determined by the Akhieser loss caused by relaxation of the thermal phonon distribution toward equilibrium [3.1]. Woodruff and Ehrenreich [3.2] have derived a formula, which describes the acoustic attenuation as a function of the cyclic acoustic frequency Ω and absolute temperature $\mathbf{T}$ and which expresses the attenuation α in nepers per unit time

$$\alpha = \frac{\mathbf{G}^2 \Omega^2 \kappa_T \mathbf{T}}{\rho \mathbf{V}^5} , \tag{3.8}$$

where $\mathbf{G}$ is the Gruneisen constant and κ_T is the adiabatic thermal conductivity. It is seen from Eq.(3.8) that the acoustic attenuation α is proportional to the squared acoustic frequency. In practice, however, it has been found that for several widely used materials the acoustic attenuation varies as $\alpha \sim \Omega^{\mathbf{m}}$, where the factor $\mathbf{m}$ lies between $\mathbf{1}$ and $\mathbf{2}$, and it can depend on the frequency range as well as on the specific sample exploited. This is a notable point especially for high-frequency acousto-optic materials where acoustic attenuation may become a major factor of limitations. Usually, however, the acoustic attenuation is most often defined as $\alpha(\mathbf{f}) = \Gamma \mathbf{f}^{\mathbf{m}}$, where Γ is the attenuation constant per unit length at the frequency $\mathbf{1\,GHz}$, $\mathbf{f} = \Omega/(2\pi)$ is the frequency in $\mathbf{[GHz]}$, and the factor $\mathbf{m}$ is a constant, which is equal to $\mathbf{2}$ for most crystals of interest. Here, one can express, for example, $\alpha(\mathbf{f})$ in $\mathbf{[dB/cm]}$ and Γ in $\mathbf{[dB/(cm \cdot GHz^2)]}$. In this case, the acoustic attenuation α measured in nepers per second in Eq.(3.8), is expressed as

$$\alpha = \frac{\Gamma \mathbf{V} \mathbf{f}^2}{\mathbf{20\,(lg\,e)}} . \tag{3.9}$$

Then, we emphasize that practically the acoustic attenuation along a propagation path is often higher then predicted by the above-noted parameters α and Γ. The additional losses may be attributed to acoustic diffraction losses, losses due to scattering from crystal impurities, acoustic beam walk-off, and acoustic harmonic losses because of acoustic nonlinearities.

The Bragg regime of light diffraction occurs with a large length $\mathbf{L}$ of interaction between light and elastic waves. In this case, the dynamic acoustic grating is rather thick, so during the analysis of diffraction one has to take into account the phase relations between waves in different orders. Such a regime can be realized only when the angle $\theta_{\mathbf{B}}$ of light incidence on a thick acoustic grating meets the Bragg conditions and $\mathbf{Q} = 2\pi\lambda \mathbf{L}/\Lambda^2 >> \mathbf{1}$ (here, λ and Λ are the light and elastic wavelengths, respectively). Usually, the Bragg regime includes one incident and two scattered light modes as well as the acoustic mode. Such a regime represents so-called one-phonon Bragg light scattering, normal or anomalous. In this regime, the scattered light intensities $\mathbf{I_0}$ and $\mathbf{I_1}$ are governed by trigonometric function dependences in the forms [3.3]

$$\text{a)}\ \mathbf{I_0} = \cos^2\left(\frac{\mathbf{q}\,\mathbf{z}}{2}\right), \qquad \text{b)}\ \mathbf{I_1} = \sin^2\left(\frac{\mathbf{q}\,\mathbf{z}}{2}\right), \qquad \text{c)}\ \mathbf{q} = \pi\,(\lambda \cos\theta_{\mathbf{B}})^{-1}\sqrt{2\mathbf{M_2}\,\mathbf{P}\,\mathbf{S}^{-1}}\,, \tag{3.10}$$

where $\mathbf{z}$ is the coordinate almost along a direction of light propagation, $\mathbf{M_2}$ is the acousto-optic figure of merit and $\mathbf{P/S}$ is the acoustic power density. Taking into account the attenuation of total energy in a volume of a deformed body, one can find both the acoustic power density and the modulation parameter $\mathbf{q}$ as

$$\text{a)}\ \frac{P}{S}=\frac{1}{2}\rho V^3 U^2 \exp(-2\alpha x)\ , \qquad \text{b)}\ q=\pi U \exp(-\alpha x)(\lambda \cos\theta_B)^{-1}\sqrt{\rho V^3 M_2}\ , \quad (3.11)$$

where U is amplitude of the elastic wave and x is the coordinate along a direction of ultrasound propagation. Usually, during the spectrum analysis the magnitude of the parameter q for each individual spectral component of a radio-signal is really small, so that one can approximate Eqs.(3.10b) and (3.10c) in the acousto-optical cell with linear acoustic losses. For the regime of a one-phonon light scattering, such an approximation can be successfully done in a vicinity of the point $qz=0$. In this case, the real-valued amplitude $E_1(x,z)$ of the scattered light field, i.e. the issuing light amplitude at the output facet of acousto-optical cell, is directly proportional to the modulation parameter q, so that one can obtain

$$\text{a)}\ E_1(x,z)=E_1(z)E_1(x)\ , \quad \text{b)}\ E_1(x)=\exp(-\alpha x)\ , \quad \text{c)}\ E_1(z)=\frac{\pi z U}{2\lambda \cos\theta_B}\sqrt{\rho V^3 M_2}\ . \quad (3.12)$$

3.3. GAUSSIAN APODIZATION OF THE INCOMING LIGHT FIELD DISTRIBUTION ALONG AN APERTURE OF THE ACOUSTO-OPTICAL CELL WITH ACOUSTIC LOSSES

Now, we make an attempt to describe the effect of apodization for the incoming light beam on the potential dynamic range of acousto-optical spectrum analyzer. To take into account the contributions from the acoustic losses we shift the origin of the physical coordinate x across a beam so that the magnitude $x=0$ will be associated with the plane of piezoelectric transducer in an acousto-optical cell. In fact, this means that we replace x by $x-0.5D$, where D is the physical cell's aperture measured in centimeters. One can suppose that the electric field amplitude profile $A(x)$, inherent in the issuing beam of a gas laser and reaching the acousto-optical cell aperture, is usually close to the Gaussian shape [3.4], see Fig.3.2a. At this step, let us put $b=0$ in that figure, so that one can write (in both real and dimensionless variables) that

$$A(x)=A_0\exp[-\sigma(x-x_0)^2]=A_0\exp[-\beta(y-0.5)^2]\ , \quad I(y)=|A_0|^2\exp[-2\beta(y-0.5)^2]\ . \quad (3.13)$$

Here, $y=x/D$ is the normalized dimensionless coordinate along the aperture D, so that $y\in\{0,1\}$, while σ and $\beta=\sigma D^2$ are physical and dimensionless input profile parameters for the Gaussian function, whose variations with the input profile parameter β are depicted in Fig.3.2.b.

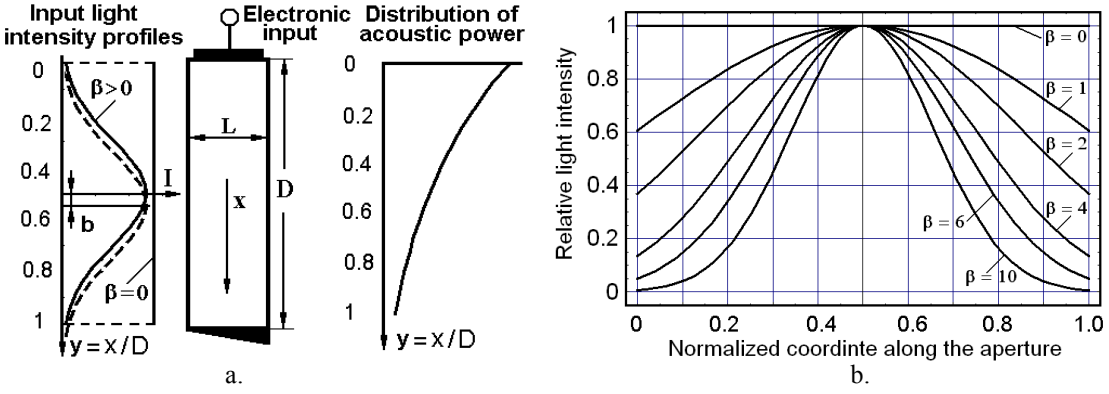

Figure 3.2. Optical arrangement of lighting the acousto-optical cell (a) and a role of the profile parameter β (b).

Taking into account the acoustic attenuation, one can find the magnitudes of the following light intensities

$$\text{a)}\ \mathbf{I_T} = \int_{-\infty}^{+\infty} \exp(-2\beta y^2)\, dy = \sqrt{\frac{\pi}{2\beta}}\ , \qquad \text{b)}\ \mathbf{I_0} = \int_{0}^{1} \exp\,[-2\beta(y-0.5)^2]\, dy = \sqrt{\frac{\pi}{2\beta}}\ \mathrm{Erf}\sqrt{\frac{\beta}{2}}\ . \quad (3.14)$$

$$\mathbf{I_A} = \int_{0}^{1} \exp\,[-2\beta(y-0.5)^2]\cdot\exp(-2\alpha_0 y)\, dy = \frac{1}{2}\sqrt{\frac{\pi}{2\beta}}\exp\left[\frac{\alpha_0(\alpha_0-2\beta)}{2\beta}\right]\cdot\left[\mathrm{Erf}\left(\frac{\alpha_0+\beta}{\sqrt{2\beta}}\right)-\mathrm{Erf}\left(\frac{\alpha_0-\beta}{\sqrt{2\beta}}\right)\right] \quad (3.15)$$

Here, the dimensionless amplitude parameter $\alpha_0 = \alpha D$ describes now the total amplitude acoustic losses along the optical aperture of a cell, because $\alpha\,[\mathrm{cm}^{-1}] = 0.115\cdot\alpha\,[\mathrm{dB/cm}]$. The ratio $\mathbf{I_A/I_T}$ represents the coefficient of utilization for the total incident light intensity $\mathbf{I_T}$. One can see from Eqs.(3.14) and (3.15) that the ratio $\mathbf{I_A/I_T}$ grows, while the absolute level $\mathbf{I_A}$ of light intensity decreases as the apodization parameter β grows, see Fig.3.3.

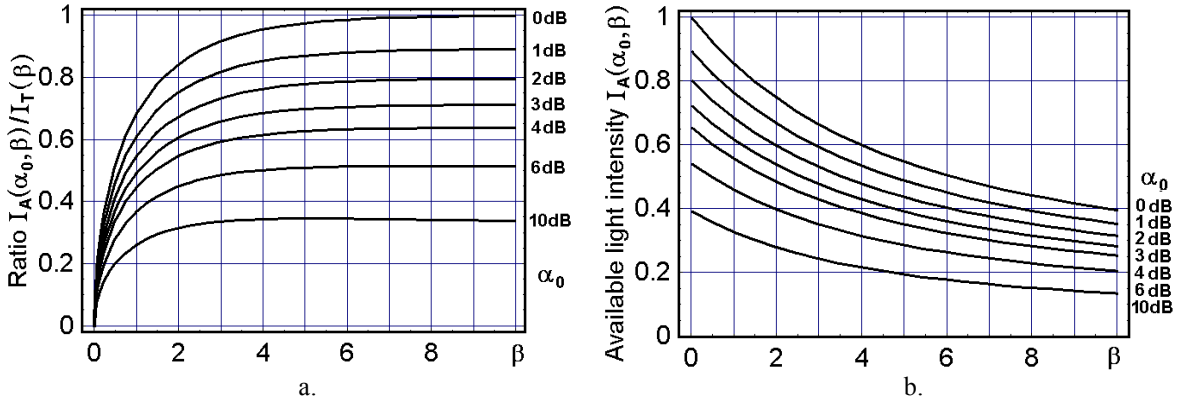

Figure 3.3. Plots of the available optical intensities: (a) the ratio $\mathbf{I_A/I_T}$ and (b) the absolute level $\mathbf{I_A}$

The shape of light field distribution $\mathbf{A(u)}$ peculiar to an individual resolvable spot in the Fourier-transform plane, i.e. in a focal plane of the integrating lens, where the spatial dimensionless coordinate $\mathbf{u}$ is centered on a maximum of that distribution, can be estimated analytically as

$$\text{a)}\ \mathbf{A(u)} = \int_{0}^{1} \exp\,[-\beta(y-0.5)^2]\ \exp(-\alpha_0 y)\ \exp(-2i\pi u y)\, dy =$$

$$= \frac{1}{2}\sqrt{\frac{\pi}{\beta}}\exp\left[\frac{(\alpha_0+2\pi i u)\cdot(\alpha_0+2\pi i u-2\beta)}{4\beta}\right]\left\{\mathrm{Erf}\left[\frac{\alpha_0+2\pi i u+\beta}{2\sqrt{\beta}}\right]-\mathrm{Erf}\left[\frac{\alpha_0+2\pi i u-\beta}{2\sqrt{\beta}}\right]\right\}, \quad (3.16)$$

$$\text{b)}\ \mathbf{A(u=0)} = \frac{1}{2}\sqrt{\frac{\pi}{\beta}}\exp\left[\frac{\alpha_0\,(\alpha_0-2\beta)}{4\beta}\right]\left\{\mathrm{Erf}\left[\frac{\alpha_0+\beta}{2\sqrt{\beta}}\right]-\mathrm{Erf}\left[\frac{\alpha_0-\beta}{2\sqrt{\beta}}\right]\right\}.$$

Using Eqs.(3.16), the normalized distribution $\mathbf{I(u)}$ of light intensity peculiar to an individual resolvable spot in a focal plane of the integrating lens can be written as

$$\mathbf{I(u)} = \mathbf{A(u)}\,\mathbf{A^*(u)}\,\mathbf{A^{-2}(u=0)}\ . \quad (3.17)$$

Generally, $\mathbf{u = w\,D/\lambda\,F_L}$, where $\mathbf{w}$ is the physical spatial coordinate in the focal plane and $\mathbf{F_L}$ is the focal distance of the integrating lens. In the particular case of $\beta \equiv 0$, Eq.(3.17) can be simplified as

$$\mathbf{I(u,\beta = 0) = \frac{\sin^2(\pi u) + \sinh^2(\alpha_0/2)}{\left[1 + (2\pi u/\alpha_0)^2\right]\,\sinh^2(\alpha_0/2)}}\ . \qquad (3.18)$$

Figure 3.4 illustrates the dependence of light intensity distributions in the Fourier transform plane using the profile parameter β as a parameter curve families for various magnitudes of the dimension-less loss factor $\alpha_0 = \alpha\,\mathbf{D}$.

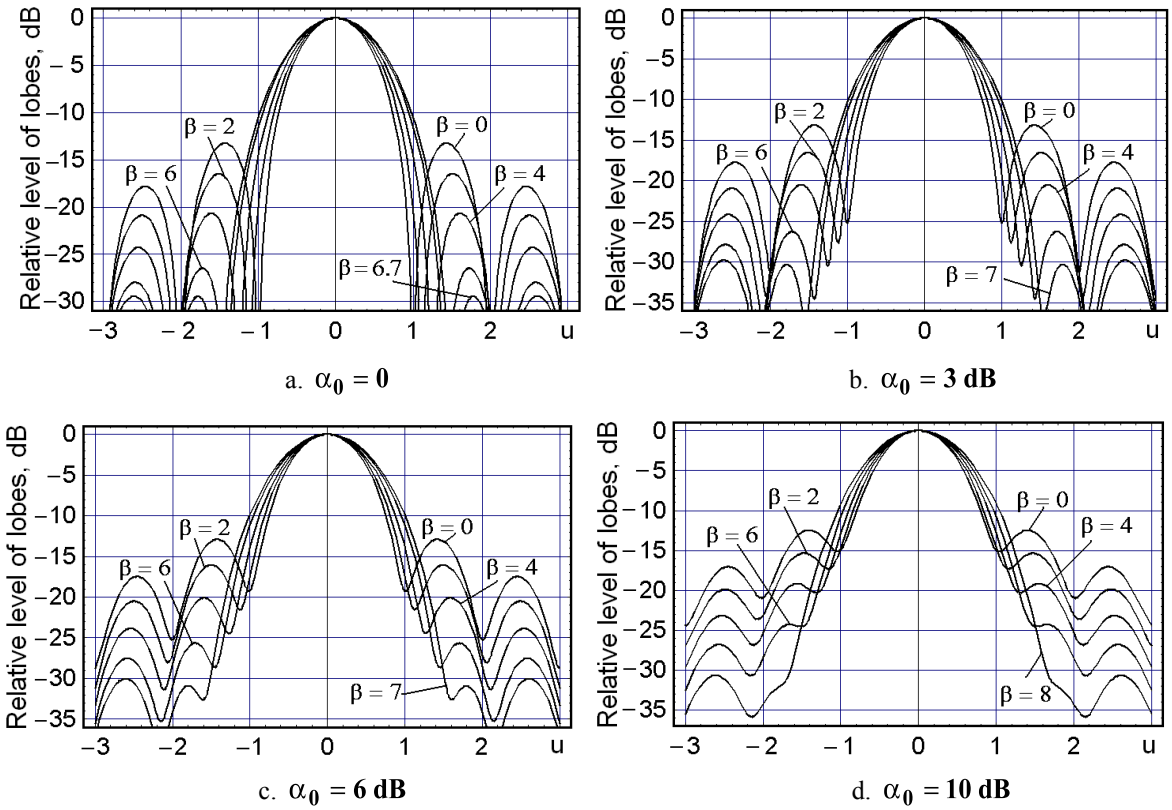

Figure 3.4. Plots of the light intensity $\mathbf{I(u)}$ for various β and α_0.

In particular, Fig.3.4a illustrates the tendencies of redistributions for light intensity profiles in the Fourier transform plane with varying the profile parameter β in a lossless regime.

3.4. SHIFTED GAUSSIAN APODIZATION OF THE INCOMING LIGHT FIELD DISTRIBUTION ALONG AN APERTURE OF THE ACOUSTO-OPTICAL CELL WITH ACOUSTIC LOSSES

Due to obvious asymmetry of the combined distribution connected with the incident Gaussian light intensity profile from a laser, which usually centered on the cell's aperture, and the acoustic power monotonously decreasing along that aperture because of losses, one can suggest shifting the incident light beam to minimize

side lobes of an individual spot in a Fourier plane. In so doing, one can modify Eq. (3.13) via introducing an additional small dimensionless parameter $\mathbf{b}$ of a shift $(|\mathbf{b}| < \mathbf{0.5})$, see Fig.3.2a, as

$$\mathbf{A(y) = A_0 \exp[-\beta (y - 0.5 + b)^2]}. \tag{3.19}$$

As a result one yields the following light intensities

$$\mathbf{a)}\ I_T = \int_{-\infty}^{\infty} \exp[-2\beta(y-0.5+b)^2]\,dy = \frac{1}{2}\sqrt{\frac{\pi}{2\beta}}\left\{ \mathrm{Erfc}\left[(1-2b)\sqrt{\frac{\beta}{2}}\right] + \mathrm{Erfc}\left[(-1+2b)\sqrt{\frac{\beta}{2}}\right]\right\},$$

$$\mathbf{b)}\ I_0 = \int_{0}^{1} \exp[-2\beta(y-0.5+b)^2]\,dy = \frac{1}{2}\sqrt{\frac{\pi}{2\beta}}\left\{ \mathrm{Erf}\left[(1+b)\sqrt{\frac{\beta}{2}}\right] + \mathrm{Erf}\left[(1-b)\sqrt{\frac{\beta}{2}}\right]\right\}, \tag{3.20}$$

$$\mathbf{c)}\ I_A = \int_{0}^{1} \exp[-2\beta(y-0.5+b)^2]\cdot\exp(-2\alpha_0 y)\,dy =$$

$$= \frac{1}{2}\sqrt{\frac{\pi}{2\beta}}\exp\left[\frac{\alpha_0(\alpha_0 - 2\beta + 4b\beta)}{2\beta}\right]\cdot\left[\mathrm{Erf}\left(\frac{\alpha_0+\beta+2b\beta}{\sqrt{2\beta}}\right) - \mathrm{Erf}\left(\frac{\alpha_0-\beta+2b\beta}{\sqrt{2\beta}}\right)\right].$$

The shape of light field distribution $\mathbf{A(u)}$ peculiar to an individual resolvable spot in the Fourier-transform plane, i.e. in a focal plane of the integrating lens where the spatial dimensionless coordinate $\mathbf{u}$ is centered on a maximum of that distribution, can be estimated analytically as

$$\mathbf{a)}\ A(u) = \int_{0}^{1} \exp[-\beta(y-0.5+b)^2]\ \exp(-\alpha_0 y)\ \exp(-2i\pi u y)\,dy =$$

$$\frac{1}{2}\sqrt{\frac{\pi}{\beta}}\exp\left[\frac{(\alpha_0+2\pi iu)\cdot(\alpha_0+2\pi iu-2\beta+4b\beta)}{4\beta}\right]\left\{\mathrm{Erf}\left[\frac{\alpha_0+2\pi iu+\beta+2b\beta}{2\sqrt{\beta}}\right] - \mathrm{Erf}\left[\frac{\alpha_0+2\pi iu-\beta+2b\beta}{2\sqrt{\beta}}\right]\right\}$$

$$\mathbf{b)}\ A(u=0) = \frac{1}{2}\sqrt{\frac{\pi}{\beta}}\exp\left[\frac{\alpha_0(\alpha_0-2\beta+4b\beta)}{4\beta}\right]\left\{\mathrm{Erf}\left[\frac{\alpha_0+\beta+2b\beta}{2\sqrt{\beta}}\right] - \mathrm{Erf}\left[\frac{\alpha_0-\beta+2b\beta}{2\sqrt{\beta}}\right]\right\}. \tag{3.21}$$

which is real-valued in behavior. Using Eqs.(3.21), the normalized distribution $\mathbf{I(u)}$ of light intensity peculiar to an individual resolvable spot in a focal plane of the integrating lens can be rewritten with Eq.(3.17). At first, it is seen from Eq.(3.17) with Eqs.(3.20) and (3.21) that the presence of a shift $\mathbf{b \neq 0}$ does not perturbed the symmetry of light distribution inherent in an individual resolvable spot in a focal plane of the integrating lens. Than, one can demonstrate that the positive shift parameter $\mathbf{b > 0}$ leads only to increasing the side lobes in comparison with the case of $\mathbf{b = 0}$, see Fig.3.5. By contrast with this, various values of the shift parameter $\mathbf{b < 0}$ make it possible both to suppress the side lobes as well as to provide higher contrast of diffractive pattern due to depressing the corresponding minima of light distribution. Figure 3.6 illustrates the dependence of light intensity distributions in the Fourier transform plane using the negative shift parameter $\mathbf{b}$ as a parameter in curve families with $\beta = 4$ for the two particular cases of the amplitude acoustic attenuation $\alpha_0 = 0.345\,(\mathbf{i.e.\ 3\ dB})$ and $\alpha_0 = 0.69\,(\mathbf{i.e.\ 6\ dB})$. However, one can see that even maximal decreasing of the side lobes, obtained through realizing similar negative shift (with $\mathbf{b = -0.04}$ for

$\alpha_0 = 0.345\,(\text{i.e. } 3\,\text{dB})$ and $b = -0.08$ for $\alpha_0 = 0.69\,(\text{i.e. } 6\,\text{dB})$), does not exceed $1\,\text{dB}$, i.e. is too insignificant. Together with this, the contrast, i.e. first minimum, can be improved from about $-32\,\text{dB}$ to about $-53\,\text{dB}$ and from about $-24\,\text{dB}$ to about $-47\,\text{dB}$, respectively.

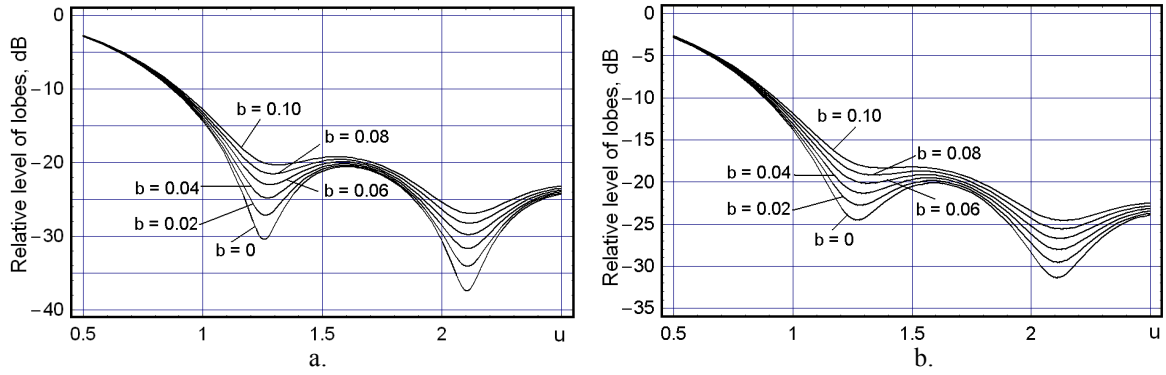

Figure 3.5. Plots of the light intensity $I(u)$ for a curve family $\beta = 4$, $b > 0$ in the particular cases: (a) $\beta = 4$, $\alpha_0 = 0.345\,(\text{i.e. } 3\,\text{dB})$ and (b) $\beta = 4$ and $\alpha_0 = 0.69\,(\text{i.e. } 6\,\text{dB})$.

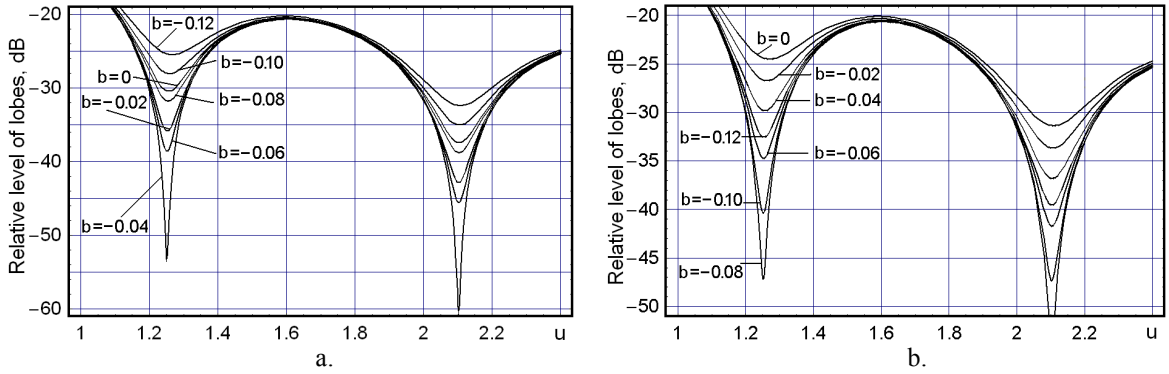

Figure 3.6. Plots of the light intensity $I(u)$ for a curve family $\beta = 4$, $b < 0$ in the particular cases: (a) $\beta = 4$, $\alpha_0 = 0.345\,(\text{i.e. } 3\,\text{dB})$ and (b) $\beta = 4$ and $\alpha_0 = 0.69\,(\text{i.e. } 6\,\text{dB})$.

4. EXPERIMENTAL CHARACTERIZATION FOR THE APODIZATION OF A LIGHT BEAM BY VARIABLE GAUSSIAN PROFILES

4.1. A MULTI-PRISM LIGHT BEAM EXPANDER

Practically important factor determining the energy in optical scheme of acousto-optical spectrometer is related to matching the initial size of laser light beam with the optical aperture of a large-aperture acousto-optical cell in the plane of light scattering. To realize a one-dimensional expanding of the laser beam together with its Gaussian apodization one can exploit a multi-prism beam expander. Such a device can be designed relatively simply and compact even with a large factor of expanding and, what is very important, can be done tunable in behavior. Using the well-known relation for the light refraction [4.1] by the first facet, i.e. the border between air and glass $\sin\varphi = n\sin\delta$, where n is the refractive index of a glass, one can obtain from Fig.4.1 the factor of spatial beam expanding in the geometrical optics approximation

$$\text{a)}\ B_1 = \frac{d_1}{d_0} = \frac{\sqrt{(n^2 - \sin^2\varphi)\,[\,1 - n^2\sin^2(\alpha-\delta)\,]}}{n\cos\varphi\cos(\alpha-\delta)}\,, \qquad \text{b)}\ \delta = \arcsin\left(\frac{\sin\varphi}{n}\right). \tag{4.1}$$

Due to the following simple relations for segments: $A_0C_0 = t_0\cdot c/n_0$, $O_0B_0 = t_0\cdot c/n_1$ and $C_1A_1 = t_1\cdot c/n_0$, $B_1O_1 = t_1\cdot c/n_1$, where t_0 and t_1 are time intervals, one can, as usually, conclude that the segments d_0, b_0 and d_1, b_1 represent in Fig.4.1 a pair of the corresponding in-phase surfaces. In the simplest case, when all the glass prisms are identical to each other and the angles φ of incidence are the same for all of them, one can write $B_m = (B_1)^m$ and obtain the needed expanding. Involving, in particular, even number m of so-called Littrow prisms (i.e. the right-angle prisms $30^0 - 60^0 - 90^0$), the beam direction can be saved with an accuracy of some spatial parallel shift, see Fig.4.2. That is why the numbers $m = \{2,4\}$ will be taken for consideration here.

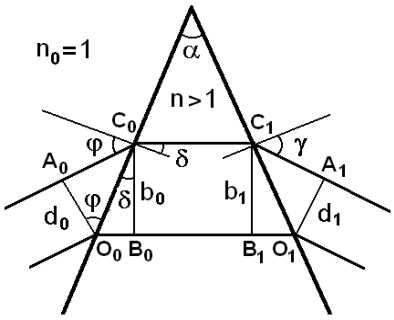

Figure 4.1. Light beam with a rectangular profile passes through an arbitrary sharp-angle prism.

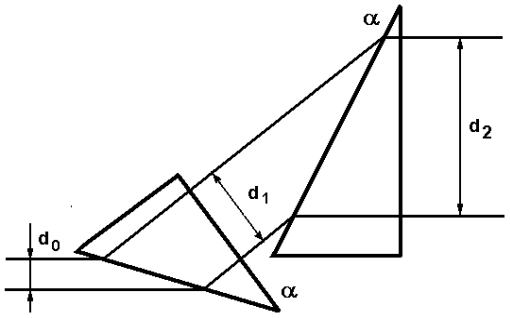

Figure 4.2. Passing the light beam with a rectangular profile through a pair $(m = 2)$ of the Littrow prisms; $\alpha = 30^0$.

Now, one has to estimate the transmittance T of a multi-prism beam expander. For this purpose, one can adapt the well-known relations for transmittance during the refraction [4.1]. These relations are depending, of course, on the chosen linear state of light polarization, so that two independent on each other linear states can be recognized, namely, the linear state of polarization being orthogonal to the plane of incidence and the

linear state of polarization belonging the plane of incidence. With these two options, for a single prism with, naturally, two borders between air and a prism material one can write

$$T_1(\perp)=\left[\frac{\sin 2\varphi \sin 2\delta}{\sin^2(\varphi+\delta)}\right]\left[\frac{\sin 2(\alpha-\delta)\sin 2\gamma}{\sin^2(\alpha-\delta+\gamma)}\right], \tag{4.2}$$

$$T_1(\parallel)=\left[\frac{\sin 2\varphi \sin 2\delta}{\sin^2(\varphi+\delta)\cos^2(\varphi-\delta)}\right]\left[\frac{\sin 2(\alpha-\delta)\sin 2\gamma}{\sin^2(\alpha-\delta+\gamma)\cos^2(\alpha-\delta-\gamma)}\right], \tag{4.3}$$

where α is the top angle of a prism, $\delta=\arcsin\left(\frac{\sin\varphi}{n}\right)$ and $\gamma=\arcsin[n\sin(\alpha-\delta)]$. One can show that $T_1(\perp)<T_1(\parallel)$ always and, consequently, $T_m(\perp)<T_m(\parallel)$ where $T_m(\perp)=[T_1(\perp)]^m$ and $T_m(\parallel)=[T_1(\parallel)]^m$. In the particular case of glass prisms with $n=1.5$ and $\alpha=30^0$, the plots characterizing the transmittances $T_m(\perp)$ and $T_m(\parallel)$ for $m=1,2,4$ are depicted in Fig.4.3. The general view of a 4-prism light beam expander is shown in Fig.4.4.

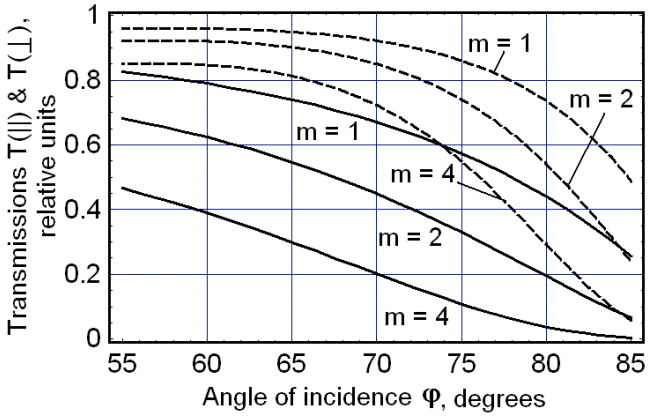

Figure 4.3. Comparison of the transmissions inherent in $m-$prism glass expanders with $n=1.5$ and $\alpha=30^0$; the solid lines are for $T_m(\perp)$, while the dashed lines are for $T_m(\parallel)$.

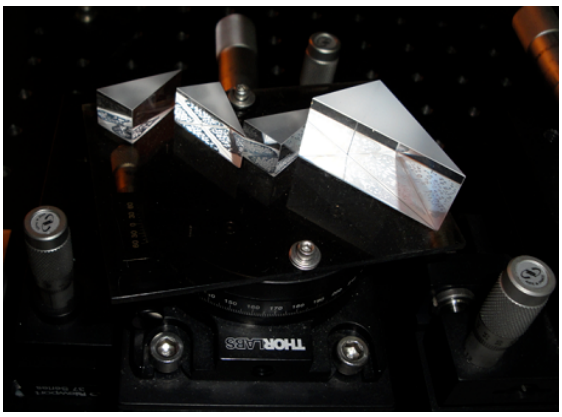

Figure 4.4. A four-prism beam expander.

The angle of light incidence on the input facet of the first prism is definitely large, about $\mathbf{70^0}$, so that the prism beam expander has different transmission for the components of light polarization oriented along the unit vectors $\vec{\mathbf{e}}_1$ and $\vec{\mathbf{e}}_2$, respectively. In fact, it plays a role of a filter, whose Jones matrix $\mathbf{M}$ can be written in the chosen axes as

$$\mathbf{M} = \begin{pmatrix} \mathbf{m_1} & \mathbf{0} \\ \mathbf{0} & \mathbf{m_2} \end{pmatrix} = \mathbf{m_1}\ \vec{\mathbf{e}}_1 \cdot \vec{\mathbf{e}}_1 + \mathbf{m_2}\ \vec{\mathbf{e}}_2 \cdot \vec{\mathbf{e}}_2\ , \tag{4.4}$$

where $\mathbf{m_{1,2}} \in \mathbf{[0,1]}$ are the transmission factors determined by properties of the beam expander. These factors can be estimated by the relations $\mathbf{m_1} = \sqrt{\mathbf{T_m(\|)}}$ and $\mathbf{m_2} = \sqrt{\mathbf{T_m(\perp)}}$. The Jones matrix $\mathbf{M}$, whose eigen-values are just $\mathbf{m_1}$ and $\mathbf{m_2}$, describes the beam expander as a filter, which affects arriving elliptical state of polarization.

4.2. PROPERTIES OF THE BEAM EXPANDER WITHIN OPERATING OVER ELLIPTICALLY POLARIZED LIGHT

In the case of optically active crystal, when normal component of the gyration tensor is non-zero, both the propagating light waves are elliptically polarized. Their ellipses of polarizations have the same relations between the corresponding axes, but these ellipses are rotated relative each other through $\mathbf{90^0}$ and traced around in the opposite directions. These two light waves can be characterized by a pair of the following complex-valued electric induction vectors

$$\text{a)}\ \vec{\mathbf{D}}^{(1)} = \mathbf{d}^{(1)}(\vec{\mathbf{e}}_1 + \mathbf{i}\rho\vec{\mathbf{e}}_2)\,, \qquad \text{b)}\ \vec{\mathbf{D}}^{(2)} = \mathbf{d}^{(2)}(\mathbf{i}\rho\vec{\mathbf{e}}_1 + \vec{\mathbf{e}}_2)\,, \tag{4.5}$$

which include a pair of the unit vectors $\vec{\mathbf{e}}_1$ and, $\vec{\mathbf{e}}_2$ as well as their joint ellipticity ρ. The ends of real-valued vectors $\mathbf{Re}\,\vec{\mathbf{D}}^{(1)}$ and $\mathbf{Re}\,\vec{\mathbf{D}}^{(2)}$ (here, $\mathbf{n_2 < n_1}$, which means that the second light wave, i.e. with the sub-index $\mathbf{"2"}$, is passing faster than the first one) represent various ellipses.

Here, a part of a scheme realizing the control over light polarization in the chosen fragment of optical system is briefly characterized. The corresponding schematic arrangement is shown in Fig.4.5; it includes only two components: a multi-prism one-dimensional beam expander and a specific acousto-optical cell made of a tellurium dioxide crystal. The problem under consideration is: "What should be the state of the initial light polarization, which incidents on the input beam expander aperture to obtain at the output of expander a pre-assigned state of light polarization, which coincides with just the eigen-state of elliptic light polarization required at the input aperture of acousto-optical cell made of optically active tellurium dioxide crystal.

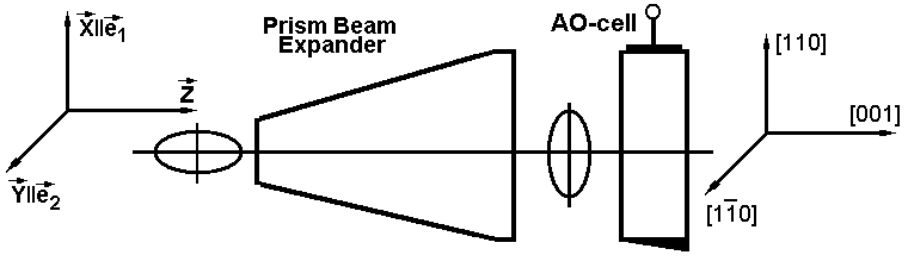

Figure 4.5. Schematic arrangement of components taken for the control over light polarization.

Let us use slightly modified technique of Jones vectors and matrices to describe states of polarization in the above-noted optical scheme, see Fig. 4.5. First of all le tus fix the laboratory coordinate system $\left(\vec{\mathbf{X}} \| \vec{\mathbf{e}}_1 ; \vec{\mathbf{Y}} \| \vec{\mathbf{e}}_2\right)$ and consider two above mentioned states of elliptic polarization with the given ellipticity. When the ellipses's major axis is lying along the $\vec{\mathbf{X}} \| \vec{\mathbf{e}}_1$ - axis, the corresponding normalizad Jones vector electric induction vector $\vec{\mathbf{D}}^{(1)}$ can be represented by $\vec{\mathbf{p}}_1 = \zeta_1 \left(\vec{\mathbf{e}}_1 + \mathbf{i}\, \rho_1\, \vec{\mathbf{e}}_2\right)$, where the mormalizing constant is $\zeta_1 = \left(1 + \rho_1^2\right)^{-1/2}$ with $\rho_1 \in [-1,1]$, see [4.2]. When visa verse the ellipse's major axis is lying along the $\vec{\mathbf{Y}} \| \vec{\mathbf{e}}_2$ - axis, the corresponding normalizad Jones vector electric induction vector $\vec{\mathbf{D}}^{(2)}$ can be represented by $\vec{\mathbf{p}}_2 = \zeta_2 \left(\mathbf{i}\rho_2 \vec{\mathbf{e}}_1 + \vec{\mathbf{e}}_2\right)$, where the normalizing constant is $\zeta_2 = \left(1 + \rho_2^2\right)^{-1/2}$ with $\rho_2 \in [-1,1]$ as well.

Now, one can suppose that, in spite of manifesting the optical activity, the axes determined by the eigen-state of elliptic light polarization coincide with crystallographic axes of tellurium dioxide single crystal installed in a cell, i.e. with a pair of axes $([110],[1\bar{1}0])$ from an axis triplet shown in Fig.4.5. In this case, one could significantly simplify the analysis, because rotating ellipses inherent in the eigen-polarizations can be omitted. In so doing, let us take, for example, the particular case of $\mathbf{m_1} > \mathbf{m_2}$ and consider this affecting for two orthogonal states of elliptic polarizations. For the unit-valued induction vector $\vec{\mathbf{D}}^{(1)}$ one yields

$$\text{a)}\ \mathbf{M}\vec{\mathbf{p}}_1 = \frac{1}{\sqrt{1+\rho_1^2}} \begin{pmatrix} \mathbf{m_1} & 0 \\ 0 & \mathbf{m_2} \end{pmatrix} \begin{pmatrix} 1 \\ \mathbf{i}\rho_1 \end{pmatrix} = \frac{\mathbf{m_1}}{\sqrt{1+\rho_1^2}} \begin{pmatrix} 1 \\ \mathbf{i}\rho_1 \dfrac{\mathbf{m_2}}{\mathbf{m_1}} \end{pmatrix} = \frac{\nu_1}{\sqrt{1+\mathbf{r}_1^2}} \begin{pmatrix} 1 \\ \mathbf{i}\mathbf{r}_1 \end{pmatrix}. \qquad (4.6)$$

A new ellipticity $\mathbf{r}_1 = \rho_1 \mathbf{m_2}/\mathbf{m_1} < \rho_1$ keeps the sign of ρ_1 due to real-valued inequality $\mathbf{m_1} > \mathbf{m_2}$ and the amplitude $\nu_1 = \mathbf{m_1}\sqrt{1+\mathbf{r}_1^2} \Big/ \sqrt{1+\rho_1^2}$ reflects losses. Thus, one can conclude that Eq.(4.6) gives a new induction vector, which is quite similar to $\vec{\mathbf{D}}^{(1)}$ in structure; with the only difference that the values of both its ellipticity $\mathbf{r}_1 > 0$ and its amplitude $\nu_1 < 1$ become smaller then ellipticity and amplitude of the vector $\vec{\mathbf{D}}^{(1)}$. For the unit-valued induction vector $\vec{\mathbf{D}}^{(2)}$ one arrives at the relation

$$\mathbf{M}\vec{\mathbf{p}}_2 = \frac{1}{\sqrt{1+\rho_2^2}} \begin{pmatrix} \mathbf{m_1} & 0 \\ 0 & \mathbf{m_2} \end{pmatrix} \begin{pmatrix} \mathbf{i}\rho_2 \\ 1 \end{pmatrix} = \frac{\mathbf{m_2}}{\sqrt{1+\rho_2^2}} \begin{pmatrix} \mathbf{i}\rho_2 \dfrac{\mathbf{m_1}}{\mathbf{m_2}} \\ 1 \end{pmatrix} = \frac{\nu_2}{\sqrt{1+\mathbf{r}_2^2}} \begin{pmatrix} \mathbf{i}\mathbf{r}_2 \\ 1 \end{pmatrix}, \qquad (4.7)$$

where $\mathbf{r}_2 = \rho_2 \mathbf{m_1}/\mathbf{m_2}$ and $\nu_2 = \mathbf{m_2}\sqrt{1+\mathbf{r}_2^2} \Big/ \sqrt{1+\rho_2^2}$. Here, two possibilities have to be analyzed. The first one appears if $|\mathbf{r}_2| \le 1$. In this case, Eq.(4.7) determines a new induction vector, which is similar to $\vec{\mathbf{D}}^{(2)}$ in structure; with the difference that the modulus of its ellipticity $\mathbf{r}_2$ exceeds $|\rho_2|$, while its amplitude decreases from initial unity to $\nu_2 < 1$. The second possibility takes place with $|\rho_2 \mathbf{m_1}/\mathbf{m_2}| > 1$, so that Eq.(4.7) should be rewritten as

$$\mathbf{M}\vec{\mathbf{p}}_2 = \frac{1}{\sqrt{1+\rho_2^2}} \begin{pmatrix} \mathbf{m_1} & 0 \\ 0 & \mathbf{m_2} \end{pmatrix} \begin{pmatrix} \mathbf{i}\rho_2 \\ 1 \end{pmatrix} = \frac{\mathbf{i}\rho_2 \mathbf{m_1}}{\sqrt{1+\rho_2^2}} \begin{pmatrix} -\mathbf{i}\dfrac{1}{\mathbf{m_2}} \\ \dfrac{}{\mathbf{m_1}\rho_2} \end{pmatrix} = \frac{\nu \cdot \exp(\mathbf{i}\pi/2)}{\sqrt{1+\mathbf{r}^2}} \begin{pmatrix} 1 \\ -\mathbf{i}\mathbf{r} \end{pmatrix}, \qquad (4.8)$$

where a new ellipticity $-\mathbf{r} = -\mathbf{m_2}/(\mathbf{m_1}\rho_2)$ is opposite in sign to ρ_2 and the amplitude factor $\nu = \mathbf{m_1}\rho_2\sqrt{1+\mathbf{r}^2}\Big/\sqrt{1+\rho_2^2}$ can include the sign of ρ_2. At this point, one can see that Eq.(4.8) illustrates converting the vector $\vec{\mathbf{D}}^{(2)}$ to the other induction vector, which has an additional phase shift by at least $\pi/2$ (may be more due to the sign of ρ_2) and is similar to $\vec{\mathbf{D}}^{(1)}$ in structure. Nevertheless, the direction of rotation inherent in each initial vector of induction will be conserved within all the cases described by Eqs.(4.6) – (4.8).

4.3. PRACTICAL EXAMPLES FOR OPERATING OVER MUTUALLY CONJUGATED EIGEN-STATES OF ELLIPTIC POLARIZATION

Let us take $\mathbf{B_4} = \mathbf{40}$ and $\rho = \mathbf{0.88}$, which both are conditioned by practically exploited tellurium dioxide acousto-optical cell. The chosen factor of expanding means, see Fig.4.3, that $\mathbf{T_4}(\|) = \mathbf{0.67}$ and $\mathbf{T_m}(\perp) = \mathbf{0.16}$, so that $\mathbf{m_1} = \mathbf{0.818}$ and $\mathbf{m_2} = \mathbf{0.400}$, i.e. $\mathbf{m_1} > \mathbf{m_2}$. Now, two particular cases appear for the analysis in details.

Case 1: Let us suppose that one has already obtained one of the pre-scripted elliptic eigen-states of polarization, whose Jones vector looks like: $\vec{\mathbf{q}}_1 = \nu_1\,(1+0.88^2)^{-1/2}\begin{pmatrix}1\\ \mathbf{i}\cdot\delta\cdot\mathbf{0.88}\end{pmatrix}$, where ν_1 is the complex-valued coefficient, reflecting optical losses and phase shift produced by that filter, and $\delta = \pm\mathbf{1}$ is the sign factor. To find the needed initial state of polarization applied at the input facet of beam expander one has to consider the process of shaping this eigen-state in the opposite direction, i.e. exploit the inverse matrix $\mathbf{M}^{-1}$ of amplitude coefficients to the matrix $\mathbf{M}$. Using Eq.(4.4) and ratio $\mathbf{M}^{-1} = \tilde{\mathbf{M}}/(\det\mathbf{M})$, where $\tilde{\mathbf{M}}$ is the matrix of algebraic complements, one can find that $\mathbf{M}^{-1} = \mathbf{m_1}^{-1}\,\vec{\mathbf{e}}_1\cdot\vec{\mathbf{e}}_1 + \mathbf{m_2}^{-1}\,\vec{\mathbf{e}}_2\cdot\vec{\mathbf{e}}_2$ and write

$$\mathbf{M}^{-1}\vec{\mathbf{q}}_1 = \frac{\nu_1}{\sqrt{1+\mathbf{0.88}^2}}\begin{pmatrix}\mathbf{m_1}^{-1} & \mathbf{0}\\ \mathbf{0} & \mathbf{m_2}^{-1}\end{pmatrix}\begin{pmatrix}1\\ \mathbf{i}\delta\cdot\mathbf{0.88}\end{pmatrix} = \frac{\nu_1}{\sqrt{1+\mathbf{0.88}^2}}\begin{pmatrix}\mathbf{m_1}^{-1}\\ \mathbf{i}\delta\cdot\mathbf{m_2}^{-1}\cdot\mathbf{0.88}\end{pmatrix}. \tag{4.9}$$

There are two options how to normalize the obtained Jones vector in the right hand side of Eq.(4.9). If one will factor out the term $\mathbf{m_1}^{-1}$, he yields $\mathbf{M}^{-1}\vec{\mathbf{q}}_1 \sim \begin{pmatrix}1\\ \mathbf{i}\delta\cdot(\mathbf{m_1}/\mathbf{m_2})\cdot\mathbf{0.88}\end{pmatrix}$ with $(\mathbf{m_1}/\mathbf{m_2})\cdot\mathbf{0.88} > \mathbf{1}$. However, this inequality is unacceptable, so that one should consider the other option for normalization and factor out the term $(\mathbf{i}\delta\cdot\mathbf{m_2}^{-1}\cdot\mathbf{0.88})$ in the right hand side of Eq.(4.9). As a result, one will arrive at the following initial state of polarization

$$\mathbf{M}^{-1}\vec{\mathbf{q}}_1 = \frac{\mathbf{i}\delta\cdot\nu_1\cdot\mathbf{0.88}}{\mathbf{m_2}\sqrt{1+\mathbf{0.88}^2}}\begin{pmatrix}-\mathbf{i}\delta\cdot(\mathbf{m_2}/(\mathbf{m_1}\cdot\mathbf{0.88}))\\ \mathbf{1}\end{pmatrix} = \frac{\mathbf{1}}{\sqrt{1+\mathbf{0.5557}^2}}\begin{pmatrix}-\mathbf{i}\delta\cdot\mathbf{0.5557}\\ \mathbf{1}\end{pmatrix} = \vec{\mathbf{p}}_1 \tag{4.10}$$

with $\mathbf{m_2}/(\mathbf{m_1}\cdot\mathbf{0.88}) = \mathbf{0.5557}$ and $\nu_1 = (-\mathbf{i}\delta)\cdot\mathbf{0.5292}$, which has to be applied at the input facet of beam expander. To check this result one can consider the process of shaping this eigen-state in the directly, i.e. exploit the vector $\vec{\mathbf{p}}_1$ and the matrix $\mathbf{M}$ as

$$\mathbf{M}\vec{\mathbf{p}}_1 = \frac{1}{\sqrt{1+0.5557^2}}\begin{pmatrix} m_1 & 0 \\ 0 & m_2 \end{pmatrix}\begin{pmatrix} -i\delta\cdot 0.5557 \\ 1 \end{pmatrix} = \frac{1}{\sqrt{1+0.5557^2}}\begin{pmatrix} -i\delta m_1\cdot 0.5557 \\ m_2 \end{pmatrix}. \qquad (4.11)$$

There are two ways for the normalizing the Jones vector in the right hand side of Eq.(4.11). If one will factor out the term m_2, he can find $\mathbf{M}\vec{\mathbf{p}}_1 \sim \begin{pmatrix} -i\delta(m_1/m_2)\cdot 0.5557 \\ 1 \end{pmatrix}$ with $(m_1/m_2)\cdot 0.5557 > 1$. However, this inequality is unacceptable, so that one should consider the other option for normalization and factor out the term $(i\delta\cdot m_1\cdot 0.5557)$ in the right hand side of Eq.(4.11). Consequently, one will have found the following final state of elliptic polarization

$$\mathbf{M}\vec{\mathbf{p}}_1 = \frac{-i\delta\cdot m_1\cdot 0.5557\cdot\sqrt{1+0.88^2}}{\sqrt{1+0.5557^2}}\cdot\frac{1}{\sqrt{1+0.88^2}}\cdot\begin{pmatrix} 1 \\ \dfrac{i\delta\cdot m_2}{m_1\cdot 0.5557} \end{pmatrix} = \frac{-i\delta\cdot 0.5292}{\sqrt{1+0.88^2}}\begin{pmatrix} 1 \\ i\delta\cdot 0.88 \end{pmatrix} = \vec{\mathbf{q}}_1, \qquad (4.12)$$

which is perfectly similar to the above-mentioned pre-scripted state with $\nu_1 = (-i\delta)\cdot 0.5292$ in the **case no.1**.

Case 2: Now, in the same way as before, one can consider the already obtained pre-scripted elliptic eigen-states of polarization at the output facet of the expander. Let its Jones vector is given by $\vec{\mathbf{q}}_2 = \nu_2\,(1+0.88^2)^{-1/2}\begin{pmatrix} i\cdot\delta\cdot 0.88 \\ 1 \end{pmatrix}$, where again ν_2 has a meaning of is the complex-valued coefficient, reflecting optical losses and phase shift produced by that filter for the other state of elliptic polarization. To determine the required initial state of polarization at the input facet of beam expander one can use the previous scheme, i.e. analyze appearing this eigen-state in the opposite direction via applying the inverse matrix $\mathbf{M}^{-1}$. Using again $\mathbf{M}^{-1} = m_1^{-1}\,\vec{e}_1\cdot\vec{e}_1 + m_2^{-1}\,\vec{e}_2\cdot\vec{e}_2$ one will have

$$\mathbf{M}^{-1}\vec{\mathbf{q}}_2 = \frac{\nu_2}{\sqrt{1+0.88^2}}\begin{pmatrix} m_1^{-1} & 0 \\ 0 & m_2^{-1} \end{pmatrix}\begin{pmatrix} i\delta\cdot 0.88 \\ 1 \end{pmatrix} = \frac{\nu_2}{\sqrt{1+0.88^2}}\begin{pmatrix} i\delta\cdot m_1^{-1}\cdot 0.88 \\ m_2^{-1} \end{pmatrix}. \qquad (4.13)$$

If one will factor out the term m_2^{-1} in the right hand side of Eq.(4.13), he yields $\mathbf{M}^{-1}\vec{\mathbf{q}}_2 \sim \begin{pmatrix} i\delta\cdot(m_2/m_1)\cdot 0.88 \\ 1 \end{pmatrix}$ with $(m_2/m_1)\cdot 0.88 = 0.4303 < 1$, which is quite acceptable in this case in contrast to the previous one. That is why the required initial state of polarization is given by

$$\mathbf{M}^{-1}\vec{\mathbf{q}}_2 = \frac{\nu_2\sqrt{1+0.43^2}}{m_2\sqrt{1+0.88^2}}\cdot\frac{1}{\sqrt{1+0.43^2}}\begin{pmatrix} i\delta\cdot 0.43 \\ 1 \end{pmatrix} = \frac{1}{\sqrt{1+0.43^2}}\begin{pmatrix} i\delta\cdot 0.43 \\ 1 \end{pmatrix} = \vec{\mathbf{p}}_2 \qquad (4.14)$$

with the real-valued $\nu_2 = 0.4894$, which has to be directed to the input facet of beam expander. To check this result one can consider the process of shaping this eigen-state in the directly, i.e. exploit the vector $\vec{\mathbf{p}}_2$ and the matrix $\mathbf{M}$ as

$$\mathbf{M}\vec{\mathbf{p}}_2 = \frac{1}{\sqrt{1+0.43^2}}\begin{pmatrix} m_1 & 0 \\ 0 & m_2 \end{pmatrix}\begin{pmatrix} i\delta\cdot 0.43 \\ 1 \end{pmatrix} = \frac{1}{\sqrt{1+0.43^2}}\begin{pmatrix} i\delta\cdot m_1\cdot 0.43 \\ m_2 \end{pmatrix}. \qquad (4.15)$$

Factor out the term $\mathbf{m_2}$, one can find $\mathbf{M}\vec{\mathbf{p}}_2 \sim \begin{pmatrix} \mathbf{i}\delta\cdot(\mathbf{m_1}/\mathbf{m_2})\cdot\mathbf{0.43} \\ \mathbf{1} \end{pmatrix}$ with $(\mathbf{m_1}/\mathbf{m_2})\cdot\mathbf{0.43} = \mathbf{0.87935} \approx \mathbf{0.88} < \mathbf{1}$, which is desirable. Consequently, one will have found the following final state of elliptic polarization

$$\mathbf{M}\vec{\mathbf{p}}_2 = \frac{\mathbf{m_2}\cdot\sqrt{\mathbf{1}+\mathbf{0.88}^2}}{\sqrt{\mathbf{1}+\mathbf{0.43}^2}}\cdot\frac{\mathbf{1}}{\sqrt{\mathbf{1}+\mathbf{0.88}^2}}\cdot\begin{pmatrix}\mathbf{i}\delta\cdot\mathbf{0.88}\\ \mathbf{1}\end{pmatrix} = \frac{\mathbf{0.4894}}{\sqrt{\mathbf{1}+\mathbf{0.88}^2}}\cdot\begin{pmatrix}\mathbf{i}\delta\cdot\mathbf{0.88}\\ \mathbf{1}\end{pmatrix} = \vec{\mathbf{q}}_2, \qquad (4.16)$$

which is perfectly the same as the above-taken pre-scripted state in the **case no.2**.

These estimations can be illustrated by results of the corresponding experimental verifications using a four-prism beam expander shown in Fig.4.4. In so doing, let us take, for example, the **case no.2** for both the values of the parameter δ. Figure 4.6 is related to realizing experimentally the output eigen-state of elliptic clockwise rotating polarization with $\delta = +\mathbf{1}$ and $\rho = +\mathbf{0.88}$. To obtain such a result presented in Fig.4.6b, the input elliptic clockwise rotating polarization with $\delta = +\mathbf{1}$ and $\rho = +\mathbf{0.43}$ had been shaped, see Fig.4.6a. To realize the output eigen-state of elliptic counter-clockwise rotating polarization with $\delta = -\mathbf{1}$ and $\rho = -\mathbf{0.88}$, see Fig.4.7b, the input elliptic counter-clockwise rotating polarization with $\delta = -\mathbf{1}$ and $\rho = -\mathbf{0.43}$ had been formed, see Fig.4.7a

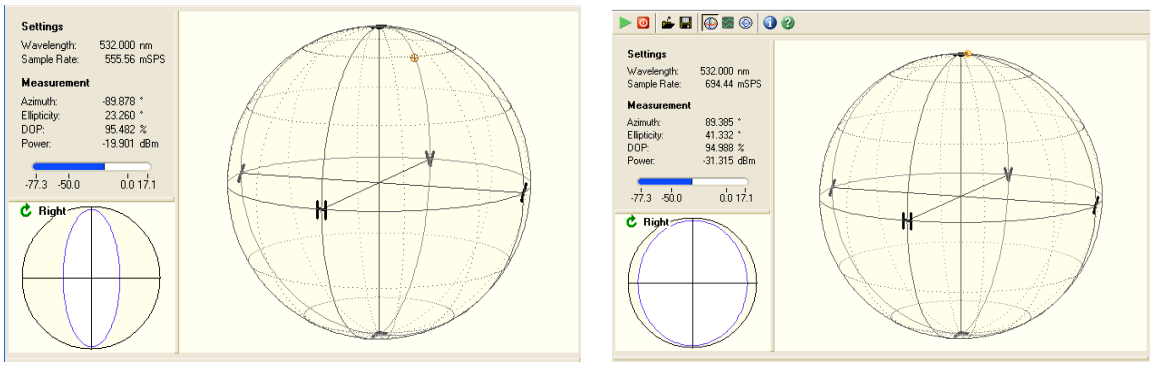

a. **b.**

Figure 4.6. Experimental data in the case **no.2** with $\delta = +\mathbf{1}$: (a) $\rho = +\mathbf{0.43}$ and (b) $\rho = +\mathbf{0.88}$ **.**

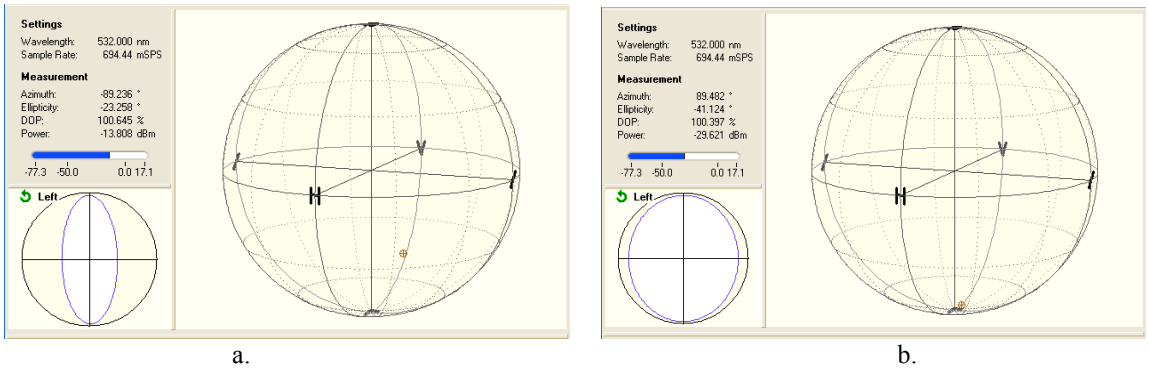

a. b.

Figure 4.7. Experimental data in the case no.2 with $\delta = -\mathbf{1}$: (a) $\rho = -\mathbf{0.43}$ and (b) $\rho = -\mathbf{0.88}$.

4.4. AN OPPORTUNITY FOR GAUSSIAN APODIZATION BY A MULTI-PRISM EXPANDER

Then, Eq.(4.1) means that initially in-phase beam with a Gaussian intensity profile, whose full width can be estimated at a given level (for instance, at a level of $\mathbf{e^{-1}}$), will be expanded by a suitable prism in the same proportion $\mathbf{B_m = d_m / d_0}$ on the given intensity level as well due to using an approximation of the geometrical optics, see Fig.4.8.

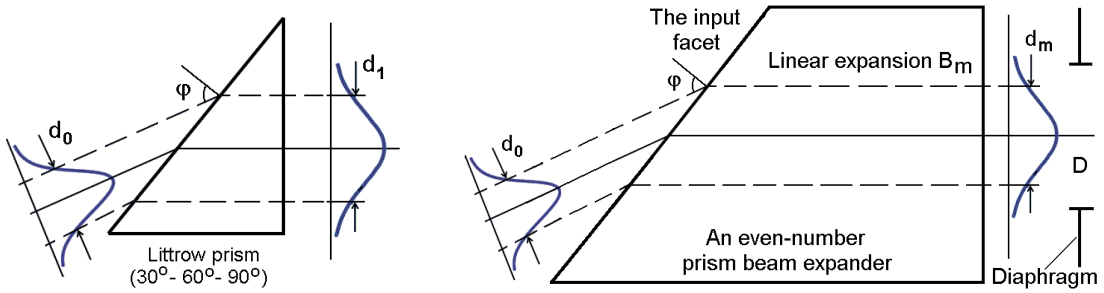

Figure 4.8. An infinite Gaussian profile passing through a single Littrow prism (a) and an expander with a diaphragm (b).

Equation (4.1) determines practically important dependence of $\mathbf{B_m}$ and $\mathbf{d_m}$ on the angle φ of light incidence on the input facet of a beam expander. The plot describing the linear beam expansion by two sets including $\mathbf{m = \{2,4\}}$ equivalent Littrow prisms with $\mathbf{n = 1.5}$ and $\alpha = \mathbf{30^0}$ are presented in Fig.4.9. It is seen that the corresponding angles φ of incidence become to be rather large for $\mathbf{B_m}$ lying for example, in a range of $\{\mathbf{20-60}\}$.

Let the normalized initial light intensity distribution for Gaussian beam in physical coordinates is characterized by $\mathbf{I_{in} = \exp(-2\sigma_0 x_0^2)}$, so that an intensity level of $\mathbf{e^{-1}}$ can be reached at $\mathbf{2\sigma_0 x_0^2 = 1}$, i.e. at $\mathbf{x_0 = 1/\sqrt{2\sigma_0}}$. The full width of this beam at a level of $\mathbf{e^{-1}}$ is equal to $\mathbf{d_0 = 2x_0 = \sqrt{2/\sigma_0}}$, while $\mathbf{\sigma_0 = 2/d_0^2}$. If now this beam will be expanded by $\mathbf{B_m = d_m / d_0}$ times, one can write the output light intensity distribution $\mathbf{I_{out} = \exp(-2\sigma_m x_m^2)}$ and then obtain $\mathbf{x_m = B_m x_0}$, $\mathbf{\sigma_m = 2/d_m^2 = 2/(B_m^2 d_0^2)}$, and $\mathbf{d_m = 2x_m = \sqrt{2/\sigma_m}}$. After that one can take into account the diaphragm, whose window is equal to $\mathbf{D}$ in physical coordinates, and then introduce the normalized coordinates $\mathbf{y_0 = x_0 / d_0}$ and $\mathbf{y_m = x_m / D}$. In so doing, one yields $\mathbf{I_{in} = \exp(-2\beta_0 y_0^2)}$ and $\mathbf{I_{out} = \exp(-2\beta_m y_m^2)}$, where $\mathbf{\beta_0 = \sigma_0 d_0^2 = 2}$ is the input factor and $\mathbf{\beta_m = \sigma_m D^2 = 2D^2/d_m^2}$ is the apodization factor. One can see that $\mathbf{\beta_m = 2}$ with $\mathbf{d_m = D}$ providing an intensity level of $\mathbf{e^{-1}}$.Then, one can explain the apodization factor as $\mathbf{\beta_m = 2(D^2/d_0^2)\cdot(d_0^2/d_m^2) = 2d^2/B_m^2}$, where the ratio $\mathbf{d = D/d_0}$ represents the relative output diaphragm. Dependences of the apodization factor $\mathbf{\beta_m}$ on the linear expansion $\mathbf{B_m}$ for various magnitudes of the relative output diaphragm $\mathbf{d}$ are shown in Fig.4.10. It is seen that, when $\mathbf{d^2 = B_m^2}$, every time one arrive s naturally at $\mathbf{\beta_m = 2}$.

The illustrating experimental studies on expanding the laser beam with $\mathbf{d_0 \approx 1\ mm}$ and the output diaphragm with $\mathbf{D = 20\ mm}$, providing the relative output diaphragm $\mathbf{d = D/d_0 \approx 20}$, had been carried out using a two-prism beam expander $\mathbf{(m = 2)}$ with tunable value $\mathbf{B_2}$, i.e. for various magnitudes of the apodization factor $\beta_2 \equiv \beta$. The corresponding traces presenting the light distributions along the fixed window of the output diaphragm, obtained from a 3000 pixel CCD camera (LC1-USB, Thorlabs Inc.) are shown in Fig.4.11 in absolute units (linear scale; zero level is presented) as well as in the normalized relative units. The corresponding theoretical plots are depicted in Fig.4.12.

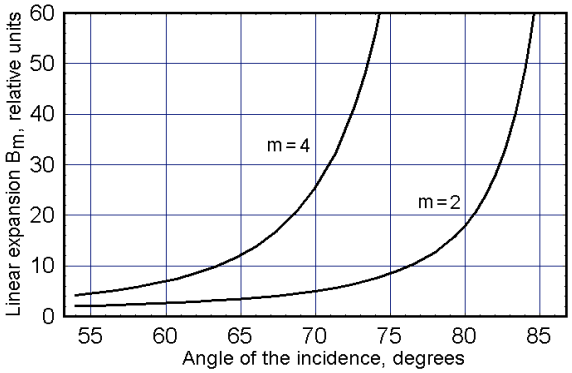

Figure 4.9. Linear expansion $\mathbf{B_m}$ providing by two sets of the prisms with $\mathbf{m = \{2,4\}}$, $\mathbf{n = 1.5}$, and $\alpha = \mathbf{30^0}$.

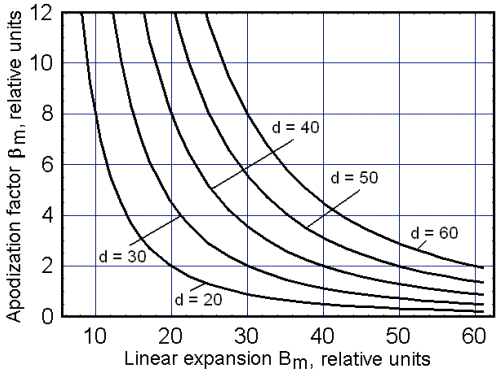

Figure 4.10. Apodization factor β_m versus the $\mathbf{B_m}$ for various relative output diaphragms $\mathbf{d}$.

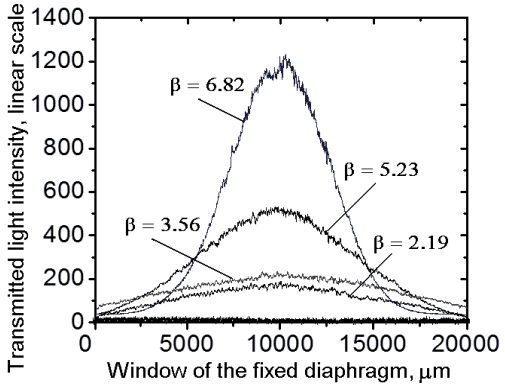

a.

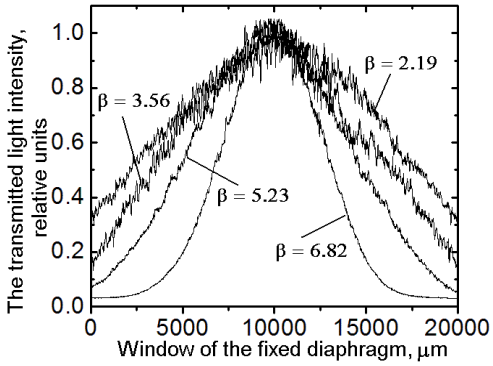

b

Figure 4.11. Experimental distributions for the transmitted light intensity along the fixed $\mathbf{20\ mm}$-window of the output diaphragm for various magnitudes of the apodization factor $\beta_2 \equiv \beta$:
(a) in absolute units (linear scale; zero level is presented) and (b) in the normalized relative units.

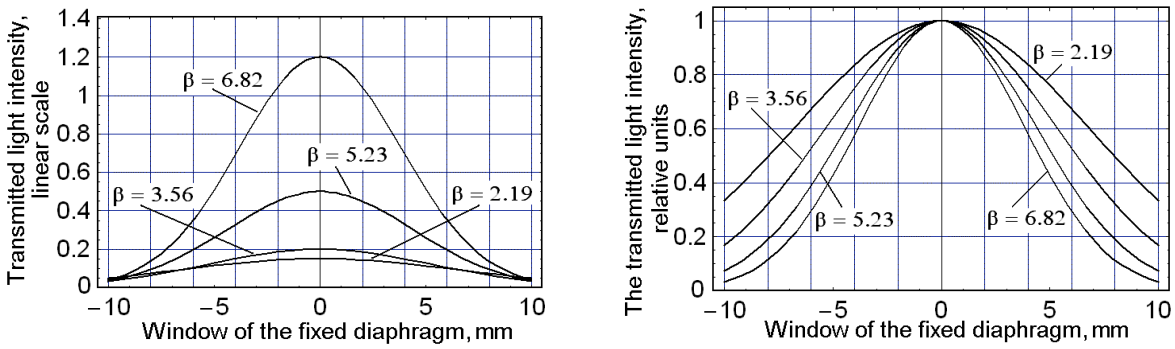

a. **b**

Figure 4.12. Theoretical plots for the transmitted light intensity along the fixed **20 mm** -window of the output diaphragm for various magnitudes of the apodization factor $\beta_2 \equiv \beta$: (a) in absolute units (linear scale) and (b) in the normalized relative units.

5. CONCLUSION

Two important aspects of optimizing the performance data peculiar to new acousto-optical spectrometers and processors for astrophysical applications have been investigated. At first, the attention has been paid to estimating the acoustic attenuation along the aperture of solid-state crystalline acousto-optical cells and its effect on the potential variations in levels of diffractive lobes in a focal plane of the integrating lens. Then, practical capabilities of the incident light beam apodization connected with improving the dynamic range of acousto-optical spectrometer as a whole have been studied here together with the contribution from acoustic attenuation in the chosen acousto-optical cell.

The obtained description governs the combined influence of these two effects. The results of our analysis have been presented via the set of numerical simulations. These data illustrate the developed approach and make it possible both to estimate the limitations and to optimize the potential dynamic range. In acousto-optic signal processing, typically acceptable level of the acoustic losses accounts about $\mathbf{3-6\ dB}$ per the total optical aperture of a cell. Thus, the effect of acoustic losses is significant due to obvious asymmetry and non-uniformity in distribution of the acoustic energy along that aperture. By this it means that the expected non-uniformity of distributing the acoustic energy should be analyzed. In terms of suppressing the side lobes, one has to try obtaining an optimized profile of the incident light beam apodization. Here, exploiting a quasi-Gaussian profile of the incident light beam reasonably shifted relative to the center of an aperture of the acousto-optical cell with appreciable acoustic losses has been proposed and estimated. It has been shown that the adequate shift allows improving the dynamic range.

An important step in characterizing new acousto-optical systems, based on large-aperture and highly effective acousto-optical cells operating in a one-phonon Bragg regime of light scattering, has been done. Rather precise control over the incident light polarization in the scheme together with a required expanding of the incident light beam have been studied, i.e. described analytically and then estimated experimentally. Moreover, one has demonstrated that the needed light-beam apodization, suppressing side lobes within registration of each individual resolvable spot and increasing the dynamic range of spectrometer, can be in principle realized practically. However, the accuracy of the achieved light distributions should be improved and potentially confirmed via direct measurements of side-lobes.

6. ACKNOWLEDGMENTS

This work had been financially supported by the CONACyT, Mexico (projects # 61237 and # 15149) as well as by the National Institute for Astrophysics, Optics & Electronics (INAOE), Mexico within the internal Acousto-Optical Spectrometer project.

7. REFERENCES

Chapter 2

2.1 R.Truel, C.Elbaum, and B.B.Chick. *Ultrasonic Methods in Solid State Physics*. (Academic Press, New York, 1969).
2.2 L.D.Landau and G.Rumer. Absorption of sound in solids. Phys. Zs. Sovjetunion. Vol.11, 18-25(1937).
2.3 G.A.Slonimsky. Soviet Physics: Journal of Experimental and Theoretical Physics. Vol.7, 1457 (1937).
2.4 A.I.Akhieser. Soviet Physics: Journal of Experimental and Theoretical Physics. Vol.8, 1318 (1938).
2.5 J.W.Tucker and V.W.Rampton. Microwave Ultrasonics in Solid State Physics. (North-Holland Publishing Co., Amsterdam, 1972).
2.6 D. Ter Haar. *Elements of Statistical Mechanics.* (Holt,Rinehart & Winson, New-York, 1954).
2.7 L.D.Landau and E.M.Lifshits. *Theory of Elastisity, Vol.7.* (Pergamon Press, Oxford-London, 1999).
2.8 M.B.Vinogradova, O.V.Rudenko, and A.P.Sukhorukov. *Theory of Waves*. (Nauka, Moscow, 1979).

Chapter 3

3.1. A.I.Akhieser. Soviet Physics: Journal of Experimental and Theoretical Physics. Vol.8, 1318 (1938).
3.2. T.O. Woodruff and H. Ehrenreich. “Absorption of sound in insulators.” Phys. Rev., V.123, pp.1553-1559 (1961).
3.3. V.I.Balakshij,V.N.Parygin, L.E.Chirkov. [Physical Principles of Acousto-Optics]. (Radio i Svyaz, Moscow, 1985).
3.4. A.Yariv and P.Yeh. [Optical waves in crystals]. (John Willey & Sons, Inc., N.-Y., 1984)

Chapter 4

4.1. M.Born and E.Wolf. Principles of Optics. 3-d Ed. (Pergamon Press, 1970, Oxford – London), Chapter 1.
4.2. Yu.I.Sirotin and M.P.Shaskolskaya. *Fundamentals of Crystal Physics.* (Mir Publishers. Moscow. 1982).